XENON TRANSIENT STUDIES FOR A CANDU REACTOR

by

Joseph KOTLARZ, BEng.

PART B: MCMASTER (OFF-CAMPUS) PROJECT

A Report Submitted to the School of Graduate Studies

in Partial Fulfillment of the Requirements

for the Degree

Master of Engineering

Department of Engineering Physics

McMaster University

Hamilton, Ontario, Canada

August 1976

MASTER OF ENGINEERING (1976) McMaster University
Department of Engineering Physics Hamilton, Ontario

TITLE: Xenon Transient Studies for a CANDU Reactor

AUTHOR: Joseph Kotlarz, BEng. (RMC)

SUPERVISOR: Dr. V.K. Mohindra and Dr. O.A. Trojan

NUMBER OF PAGES: vi, 57

A B S T R A C T

This report studies the xenon transient behaviour in a CANDU reactor as a function of time after shutdown, start-up and power set-backs. In addition, load cycling transients were obtained for typical daily load requirements.

ACKNOWLEDGEMENTS

I wish to thank the staff of Atomic Energy of Canada Limited, Power Projects, especially the Physics and Analysis Division for their benevolent assistance in the research for this project. Special thanks to Dr. V.K. Mohindra, Dr. O.A. Trojan and Mr. M. Mamourian for their help and guidance.

TABLE OF CONTENTS

LIST OF TABLES

LIST OF FIGURES

1. INTRODUCTION

Xenon-135 is formed as a fission product both directly and by the radioactive-decay chain process shown below.

(i) Direct fission yield = 0.3%

(ii) $Te^{135} \xrightarrow{2\ min} I^{135} \xrightarrow{6.7\ h} Xe^{135} \xrightarrow{9.2\ h} Cs^{135} \xrightarrow{2\times10^{4}\ y} Ba^{135}$ (stable)

Fission yield = 6.1% (1.1)

Numerous fission products resulting from reactor operation are generally classified as having high or low absorption cross sections. These products all act as poisons during reactor operation but the low cross section fission products are usually not treated separately. On the other hand, the high absorption fission products which reach equilibrium concentrations soon after startup include Xe-135, Rh-105 and Sm-149. The latter two products having absorption cross sections much less than xenon are normally neglected when xenon effects are studied. For example, the absorption cross section of xenon is 3.5×10^{6} barns compared to that for Sm-149, 4.08×10^{4} barns.[2]

Upon shutdown, the xenon reactivity load builds up to a maximum at approximately 10 hours after shutdown and then returns to an equilibrium value after $\approx$ 36 hours.

In the case of a power setback, the xenon transients are similar to those characterizing a shutdown. The rapid increase in xenon reactivity is due to its continued production from iodine in conjunction with a decrease in neutron absorption.

The peak xenon load signifies an equality between its production and destruction. The final decrease in reactivity load is due to the xenon decay and burnup exceeding production.

Further transient studies were carried out to calculate decision and action time and to study the possibility of load cycling with adjusters. Terminology defines the nominal xenon override time as the time for the xenon to build up to the reactivity capability of the xenon override system. The "decision and action time" refers to the time available to the operator in locating the fault and taking corrective action prior to withdrawing shutoff rods.

2. THEORY

2.1 Calculation Technique

Fast and thermal neutron flux distributions were calculated by solving the two-group, two-dimensional neutron diffusion equations. The steady-state diffusion equations are given below.

Fast-Group: $$\nabla^2\phi_1 - \phi_1/L_s^2 + \frac{1}{k_{eff}} \cdot \frac{k_\infty}{p} \cdot \frac{D_2}{D_1} \cdot \frac{1}{L^2} \cdot \phi_2 = 0 \qquad (2.1.1)$$

Thermal-Group: $$\nabla^2\phi_2 - \phi_2/L^2 + p \cdot \frac{D_1}{D_2} \cdot \frac{1}{L_s^2} \cdot \phi_1 = 0 \qquad (2.1.2)$$

where subscripts 1, 2 refer to fast and thermal flux respectively, and

ϕ_i = flux

D_i = diffusion coefficient

L^2 = thermal diffusion area

L_s^2 = slowing down area

k_{eff} = effective multiplication factor

p = resonance escape probability

k_∞ = infinite multiplication constant

The above diffusion equations are solved iteratively using a finite difference technique with grid representation as shown in Figure 6. For simplicity it is assumed that the mesh spacings in the r and z direction are the same. Considering the Laplacian ∇^2 in cylindrical coordinates

$$\nabla^2 = \frac{\partial^2}{\partial r^2} + \frac{1}{r}\frac{\partial}{\partial r} + \frac{\partial^2}{\partial_z{}^2} \quad .$$

The finite difference forms from the diagram are

$$\frac{\partial^2 \phi_i}{\partial r^2} \approx (\Delta r)^{-2} \left[\phi_i(r+1,z) - 2\phi_i(r,z) + \phi_i(r-1,z)\right] \tag{2.1.3}$$

$$\frac{1}{r}\frac{\partial \phi_i}{\partial r} \approx (\Delta r)^{-2} \left[\phi_i(r+1,z) - \phi_i(r,z)\right] \tag{2.1.4}$$

and

$$\frac{\partial^2 \phi_i}{\partial z^2} \approx (\Delta z)^{-2} \left[\phi_i(r,z+1) - 2\phi_i(r,z) + \phi_i(r,z-1)\right] \tag{2.1.5}$$

Substituting these above equations into the fast and thermal group diffusion equations gives the following overall result for the fast group:

Fast-Group: $(\Delta r)^{-2}\left[\phi_1(r+1,z) - 2\phi_1(r,z) + \phi_1(r-1,z)\right] +$

$+ (\Delta z)^{-2}\left[\phi_1(r,z+1) - 2\phi_1(r,z) + \phi_1(r,z-1)\right] +$

$+ (\Delta r)^{-2}\left[\phi_1(r+1,z) - \phi_1(r,z)\right] -$

$- \phi_1(r,z)/L_s^2 + \frac{1}{k_{eff}} \cdot \frac{k_\infty}{p} \cdot \frac{D_2}{D_1} \cdot \frac{1}{L^2} \cdot \phi_2(r,z) = 0$

Simplifying, we obtain

$$\phi_1(r,z) = (\Delta r)^{-2}\left[\phi_1(r+1,z) + \phi_1(r-1,z)\right] +$$

$$+ (\Delta z)^{-2}\left[\phi_1(r,z+1) + \phi_1(r,z-1)\right] +$$

$$+ (\Delta r)^{-2}\left[\phi_1(r+1,z)\right] + KK\left[\phi_2(r,z)\right] \div$$

$$\div \left[2(\Delta r)^{-2} + 2(\Delta z)^{-2} + 2(PP)^{-2}\right] \qquad (2.1.6)$$

where

$$KK = \frac{1}{k_{eff}} \cdot \frac{k_\infty}{p} \cdot \frac{D_2}{D_1} \cdot \frac{1}{L^2}$$

and

$$(PP)^{-2} = \frac{\Delta r^2 + L^2}{2L^2\,\Delta r^2} \quad .$$

Similarly, the thermal flux reduces to

$$\phi_2(r,z) = (\Delta r)^{-2}\left[\phi_2(r+1,z) + \phi_2(r-1,z)\right] +$$

$$+ (\Delta z)^{-2}\left[\phi_2(r,z+1) + \phi_2(r,z-1)\right] +$$

$$+ (\Delta r)^{-2}\left[\phi_2(r+1,z)\right] + SS\left[\phi_1(r,z)\right] \div \qquad (2.1.7)$$

$$\div \left[2(\Delta r)^{-2} + 2(\Delta z)^{-2} + 2(TT)^{-2}\right]$$

where

$$SS = p \cdot \frac{D_1}{D_2} \cdot \frac{1}{L_s^2}$$

and

$$(TT)^{-2} = \frac{\Delta r^2 + L_s^2}{2L_s^2\ \Delta r^2}$$

Equations (2.1.6) and (2.1.7) can be solved simultaneously. The number of equations for a specified reactor grid is twice the number of mesh points involved.

In the solution of equations (2.1.6) and (2.1.7) the Liebmann Overrelaxation parameter (Beta) was used. This to accelerate the iteration process relating neighbouring fluxes by solving for new values based on old flux values. At every point (r,z) the new value of fast flux,

$$\begin{aligned} \phi_1^{n+1}(r,z) = \Bigg| \Bigg\{ & (\Delta r)^{-2} \left[\phi_1^{n}(r+1,z) + \phi_1^{n}(4-1,z)\right] + \\ & + (\Delta z)^{-2} \left[\phi_1^{n}(r,z+1) + \phi_1^{n}(r,z-1)\right] + \\ & + (\Delta r)^{-2} \left[\phi_1^{n}(r+1,z)\right] + KK\left[\phi_2^{n}(r,z)\right] \div \\ & \div \left[2(\Delta r)^{-2} + 2(\Delta z)^{-2} + 2(PP)^{-2}\right] \Bigg\} - \\ & - \phi_1^{n}(r,z) \Bigg| \ BETA + \phi_1^{n}(r,z) \end{aligned} \qquad (2.1.8)$$

replaces the old $\phi_1^{n}(r,z)$ value until the convergence criteria is met. The end of the iteration process is specified by two convergence criteria:

$$\left| \frac{\phi^{n+1} - \phi^{n}}{\phi^{n+1}} \right| \leq \epsilon \quad \text{to be satisfied at every space point}$$

and letting $\frac{1}{k_{eff}} = \lambda$,

$$\frac{\lambda^{n+1} - \lambda^{n}}{\lambda^{n+1}} \leq \epsilon^{*}.$$

ϵ^{*} is different from ϵ by a factor of almost an order of magnitude. Even though the value of λ may have converged, the flux may still be an order of magnitude away. Hence, when ϵ, signifying fractional change of flux at all points is less than or equal to this change then the solution to the flux equation is converged. In general, $1 \leq \text{BETA} \leq 2$ and is a function of the number of mesh spacings in the axial and radial directions respectively[4].

2.2 Xenon Transient Equations

Xenon concentration as a function of time depends directly upon it's loss and production rate. The production-decay chain (scheme 1.1) indicates xenon produced both by fission of U-235 (0.3%) and from iodine-135. Since the half-life of Te-135 is small the iodine concentration can be assumed to be governed by the equation

$$\frac{dC_I(t)}{dt} = -\lambda_I C_I(t) - \sigma_I C_I(t) + \gamma_I \Sigma_f \phi_2$$

and when integrated

$$C_I(t) = e^{-\lambda_I t} \gamma_I \Sigma_f \int_0^t \phi_2(t) \; e^{\lambda_I t} dt \qquad (5) \qquad (2.2.1)$$

On the other hand, xenon loss is due to absorption by thermal neutrons and it's decay to Cs-135. Equation (2.1.1) may now be written as,

$$\frac{dC_X(t)}{dt} = \nu\Sigma_f \phi_2 \gamma_{Xe} + \lambda_I C_I(t) - \lambda_X C_X(t) - \sigma_X \phi_2 C_X(t) \qquad (2.2.2)$$

where

C_X = xenon-135 concentration (atoms·cm^{-3})

C_{Xo} = equilibrium xenon-135 concentration (atoms·cm^{-3})

C_I = iodine-135 concentration (atoms·cm^{-3})

C_{Io} = equilibrium iodine concentration (atoms.cm^{-3})

ν = average number of neutrons produced per fission

γ_X = direct fission product yield of xenon-135

γ_I = direct fission product yield of iodine-135

λ_X = decay constant of xenon-135 (s^{-1})

λ_I = decay constant of iodine-135 (s^{-1})

ϕ_2 = thermal neutron flux (neutrons·cm^{-2}.s^{-1})

σ_X = thermal neutron microscopic absorption cross-section of xenon (cm^{-2})

Σ_f = macroscopic fission cross-section of fuel (cm^{-1})

$C_X(t)$ = xenon concentration (atoms-cm^{-3}) at time (t)

Σ_U = absorption cross-section of fuel (cm^{-1})

Solving (2.2.1) and (2.2.2) for equilibrium conditions (i.e.: $dC_X(t)/dt$ and $dC_I(t)/dt = 0$) gave the following results:

$$C_{X_o} = \frac{\lambda_I C_{I_o} + \gamma_X \Sigma_f \phi_2}{\lambda_X + \sigma_X \phi_2} \qquad (2.2.3)$$

and

$$C_{I_o} = \frac{\gamma_I \Sigma_f \phi_2}{\lambda_I} \quad . \qquad (2.2.4)$$

In obtaining the values of xenon and iodine concentrations at points throughout the reactor, ϕ_2 is calculated as discussed in the diffusion equations (2.1.7). Thus, by iteratively solving for the thermal flux at points throughout the reactor, the xenon and iodine concentrations are similarly correlated by making use of the thermal flux found at the point in question.

3. SETTING UP THE REACTOR MODEL

The model was based on a proposed layout of a typical CANDU reactor (shown in XYZ geometry - Figures 1, 2 and 3)[6]. The latter two figures show the locations and mesh spacings for the various reactivity devices. Advantage was taken of the reactor symmetry and only a quadrant was simulated. Figure 5 is a cylindrical (r-z geometry) transformation of Figures 2 and 3. The simulated reactor contains 740 channels, has an extrapolated length of 606 cm and a radius of 508 cm. The inner radius was selected to obtain the reference flux distribution with adjuster rods represented as discs in the r-z geometry. The outer core radius was determined by the number of channels. The model was next divided into 25 regions, each having it's own lattice parameters. Finally, using the results from a detailed 3-dimensional simulation, overall flux shape and adjuster worth was matched for the 2-dimensional case. The reactor had an overall form factor of 0.64 and an adjuster worth of 22 mk. These values were assumed adequate for the purpose of this study. The equilibrium xenon in the core was-27.7 mk. In order to obtain the prescribed adjuster worth in conjunction with the form factor, the adjuster absorption cross-section and respectively the inner core radius was altered. The adjuster

rods were represented as discs perpendicular to the fuel channels by incrementing the thermal absorption cross-sections of the adjuster rod regions. Original cell parameters for equilibrium fuel conditions were obtained from various established lattice codes (see Tables 1 and 2 for reactor parameters).

4. RESULTS

4.1 Shutdown Transients

The xenon behaviour upon shutdown is best expressed through equation (2.2.2) where

$$\nu\Sigma_f\phi_2 = 0$$

and

$$\sigma_X\phi_2 C_X(t) = 0.$$

A shutdown results in xenon no longer being burnt up nor being produced directly by fissioning even though it is still produced by the equilibrium iodine. Hence, the xenon concentration increases and then decreases due to the radioactive decay process.

Figure 7 shows the xenon transient after shutdown from 100% full power for the first 51 minutes. Curve A represents equilibrium fuel conditions at an irradiation of 1.537 n/kb. Curve B is for fresh fuel and is only used for comparison. For an adjuster worth of 22 mk, the nominal xenon override time was found to be 43.8 minutes. If fresh fuel were used, for the same adjuster worth, the nominal xenon override time is 41.4 minutes. This is due to the higher direct fission product yield of I-135. Figure 8 shows the xenon reactivity transients after instantaneous shutdown from 100%, 75%, 50% and 25% full power. In addition, a shutdown transient from 100% power was calculated using a point maximum flux of 4.74×10^{17} n/cm^2/s and the core

parameters in Table 2 (see Appendix A). In all cases, the xenon peak occurs at about 10.4 hours and varies from -108 to -23 mk respective of decreasing powers. The xenon reactivity is normalized to an equilibrium value of -27.7 mk. Comparing the simulated xenon transient with that calculated (shutdown from 100% FP), the latter is similar except that it's peak xenon reactivity is approximately 7 mk higher (in negative reactivity). This difference may be accounted for in the computational method - for example, in the point calculation the spatial dependence of xenon is ignored.

Figure 9 shows the normalized peak xenon as a function of shutdown from various power levels. This turns out to be a linear function with a slope of $\approx$ 1.1 mk per 1% FP.

4.2 Startup Transients

Figures 10A and 10B reflect startup to 100%, 90%, 85%, 75%, 50% and 25% full power. In all cases, the xenon load increases to an equilibrium value after about 52 hours of reactor operation. The rate of xenon buildup decreases with time. The original increase in xenon reactivity is due mainly to the increased I-135 concentration. Figure 11 shows the equilibrium xenon as a function of power level. For a constant increase in power, the corresponding increase in equilibrium xenon is performed at a decreasing rate. This is due to the readjustment of production and losses to an equilibrium level.

4.3 Power Setback Transients

Xenon transients were obtained for power setbacks from 100% to 75%, 50% and 25% FP (Figure 12). The curves are similar in shape to the shutdown transients however peak xenon reaches lower maximum values. For example, -33 mk at 25% FP setback down to -6 mk at 75% FP. Times of xenon maxima range from two to three hours after the power setback. Further comparison to shutdown from full power demonstrates a shorter time ($\approx$ 30 hours) required to reach equilibrium xenon. This characteristic may be explained by considering

the additional fission products built up in a shutdown from 100% FP. The spontaneous decay of this fission product to xenon-135 results in a higher reactivity maximum for shutdown from 100% FP.

Figures 13A, 13B and 13C show the transient effects of xenon, iodine and thermal flux as a function of time and radial distance in the reactor for power setback to 25%. The first plot shows the buildup of xenon to a maximum and further decrease while iodine continuously decreases and thermal flux generally follows the xenon trend. Figure 13B shows the action of the normalized xenon distribution for a setback to 25% FP. The xenon is reflective of Figure 12 where a load increases to a maximum in ≈ 3 hours and then decreases to equilibrium. In this case however, the xenon distribution decreases towards equilibrium. Similarly, Figure 13C shows the thermal flux distribution as a function of radial position and time.

The above transient results do not include the effect of any power feedback. The reactivities shown are normalized to zero at a xenon concentration in equilibrium with a maximum fuel thermal flux of 0.474×10^{18} n/cm^2/hr. Furthermore, all transients such as shutdown, startup and setbacks are assumed to happen instantaneously.

4.4 Decision and Action Time (See Figure 4 for Definition)

The reactor was shut down from full power to 1% of full power instantaneously and kept there for 42.8 minutes and then the power was raised according to the power ramp shown in Figure 14. The shutdown time was selected in such a way that at the end point of total recovery time (i.e. when the rate of change of xenon concentration was zero) all the adjusters were out of the core (see Figure 15). The reactivity was controlled by adjusting the absorption in the adjuster rod regions. The xenon buildup rate was zero at a power level of about 40% of full power. The reactor power was limited by maximum bundle power (i.e. maximum flux in the fuel).

Assuming that the time to recock SDS1 'alone' to be 5 minutes and the time to withdraw the adjuster rods to be 7 minutes, the decision and action time was estimated to be 30.8 minutes. It was estimated that the D & A time could change by 5 to 10% for a more realistic 3D simulation of the reactor including the feedback reactivity effect due to power changes, zone worths, and moderator temperature change, etc. All these fine points were neglected in the present study.

4.5 Load Cycling

Two different modes of load cycling (characteristic of Figures 16A and 16B) were simulated. Both Figures 16A and 16B simulate a daily cycle of 18 hours at 100% followed by 6 hours at 50% FP. Figure 16A ignores the power coefficient while 16B includes it. Two types of plots are involved within each of the above figues - i) at a power ramp of 10% per minute, and ii) at power ramp 5% per minute. These curves are practically identical which is expected since one power ramp is the interpolated effect of the other. The plots reflect power level, form factor and xenon reactivity for the different power ramps. Criticality was maintained by adjusting the abosrption cross-section in the adjuster rod regions. The curves in Figures 16A and 16B are similar except that with the power coefficient included.

The slack in the form factor after 100% power is due to the adjustment of thermal absorption in the adjuster rod regions to compensate for the decrease in reactivity due to xenon. The reactivity during this power change course goes from a minimum of -14.5 mk to a maximum of + 4 mk and then slowly drops to an equilibrium value. In reality, poison would be added to the moderator to maintain criticality.

The second load cycle consisted of a ramp down from 100% to 65% at 7% per minute followed by 6 hours at 65% full power and then a ramp up to 100% in five minutes at 7% per minute. Figures 17A and 17B show these transients along with xenon reactivity and form factor plots. The former figure ignores the power coefficient while the latter figure includes it.

Both figures reflect two periods totalling 48 hours. Similarities in both shape and values exist between cycles 1 and 2 as shown. The reactivity due to xenon oscillates between limits of -7.3 mk to +3.2 mk when the reactivity feedback due to power coefficient was included and between limits -8.3 mk to +3.2 mk (relative to base load operation) when the effect of power coefficient on load cycle was ignored. The final load cycle consisted of $\sim$ 18 hours at 100% full power followed by six hours at 90% full power. The results are shown in Figure 18.

5. CONCLUSIONS

From a general view, the two-dimensional r-z model was adequate to show the relative effects of xenon transients. However, due to it's limitations, accurate bundle and channel powers cannot be ascertained. A detailed three-dimensional simulation is required to study accurately the changes in form factor and xenon reactivity due to discrete movement of adjuster rod banks.

APPENDIX A

EQUILIBRIUM XENON POISONING AFTER SHUTDOWN COMPUTATION

In conjunction with the xenon transient equations from section 2, the following is a sample computation for equilibrium xenon concentration and reactivity load.

$$X_o = \frac{(\gamma_i + \gamma_x)\ \Sigma_f\ \phi}{\lambda^*} \tag{1}$$

where

$$\lambda_x^* = \lambda_x + \sigma_x \phi$$

and

$$I_o = \frac{\gamma_I\ \Sigma_f\ \phi}{\lambda_I^*}$$

where

$$\lambda_I^* = \lambda_I + \sigma_I\ \phi$$

but since σ_I is very small I_o may be approximated by

$$\frac{\gamma_I\ \Sigma_f\ \phi}{\lambda_I} \quad . \tag{2}$$

Lattice Code Parameters

σ_x = 2.3762969 x 10^{18} cm^2 (temperature corrected)

$\phi_{maximum}$ = 4.7405 x 10^{17} $n/cm^2/hr$

Σ_f = 0.001805513 cm^{-1}

$$\lambda_I = 0.1034 \text{ hr}^{-1}$$

$$\lambda_x = 0.0756 \text{ hr}^{-1}$$

$$\gamma_I = 0.062059$$

$$\gamma_x = 0.005286$$

By substituting the above into equations (1) and (2)

$$x_o = 4.7488 \times 10^{13} \text{ cm}^{-3}$$

and

$$I_o = 5.1344 \times 10^{14} \text{ cm}^{-3}$$

To convert the xenon concentration to mk units,

$\rho(\text{mk}) = \dfrac{C_x(t)\,\sigma_x}{\Sigma a} = \underline{+ 28.7 \text{ mk}}$ for the case of equilibrium xenon.

Finally, a numerical expression to find the xenon concentration at time "t" after shutdown:

$$C_x(t) = \frac{\lambda_I}{\lambda_x - \lambda_I} I_o \left(e^{-\lambda_I t} - e^{-\lambda_x t}\right) + x_o e^{-\lambda_x t} \qquad (3)$$

and for this reactor model,

$$\underline{C_x(t) = -1.9097 \times 10^{15} \left(e^{-.1034t} - e^{-10756t}\right) + 4.7488 \times 10^{13}\, e^{-.0756t}} \qquad (4)$$

TABLE 1

Equilibrium Core Conditions

Average Exit Burnup	1.537 n/kb
Overall Form Factor	0.639
Load Due to Adjusters	-22 mk
Number of Active Channels	740
Zone Controllers	ignored

TABLE 2

LATTICE PARAMETERS

(Reference POWDERPUFS-V FMPAV-02 Ext. 1)

CORE PROPERTIES

k_∞	(xenon free)	1.070148	
L^2	(xenon free)	242.094	cm^2
L_s^2	(xenon free)	156.0	cm^2
p	(xenon free)	.906481	
D_1	(xenon free)	1.27294	cm
D_2	(xenon free)	0.94131	cm
$\hat{\Sigma}_a^{fuel}$		0.209924	cm^{-1}
$\hat{\Sigma}_f^{fuel}$		0.097036	cm^{-1}
f (thermal utilization)		0.939213	
ϕ_2 (maximum thermal flux in fuel)		0.47405×10^{18}	$n/cm^2/hr$

REFLECTOR PROPERTIES

L_s^2	129.8	cm^2
L^2	10470.0	cm^2
D_1	1.316	cm
D_2	0.8769	cm

XENON PARAMETERS

Infinite Xenon Load	30.95	mk
$\bar{\gamma}_I$	0.062057	
$\bar{\gamma}_{xe}$	0.005286	
λ_I	0.1034	hr^{-1}
λ_{xe}	0.0756	hr^{-1}

Note: The incremental thermal absorption cross-section used to represent the adjuster rods shown in Figure 1 was 0.0029 cm^{-1}.

TABLE 3A

Shutdown from 25% Full Power

δT(hours)	T(hours after shutdown)	-Reactivity (mk)
0.5	0.5	3.33
0.5	1.0	6.28
1.0	2.0	11.22
2.0	4.0	17.92
4.0	8.0	22.68
4.0	12.0	20.96
4.0	16.0	16.25
4.0	20.0	10.43
4.0	24.0	4.56
4.0	28.0	0.85
4.0	32.0	-5.57
4.0	36.0	-9.54

TABLE 3B

Shutdown from 50% Full Power

δT(hours)	T(hours after shutdown)	-Reactivity (mk)
0.5	0.5	7.38
0.5	1.0	13.94
1.0	2.0	24.87
2.0	4.0	39.90
4.0	8.0	52.28
4.0	12.0	51.68
4.0	16.0	44.95
4.0	20.0	35.66
4.0	24.0	25.77
4.0	28.0	16.37
4.0	32.0	7.98
4.0	36.0	0.80
4.0	40.0	-5.17
4.0	44.0	-10.02
4.0	48.0	-13.90

TABLE 3C

Shutdown from 75% Full Power

δT(hours)	T(hours after shutdown)	-Reactivity (mk)
0.5	0.5	11.46
0.5	1.0	21.54
1.0	2.0	38.22
2.0	4.0	60.91
4.0	8.0	80.00
4.0	12.0	80.51
4.0	16.0	72.26
4.0	20.0	60.14
4.0	24.0	46.89
4.0	28.0	34.02
4.0	32.0	22.35
4.0	36.0	12.23
4.0	40.0	3.73
4.0	44.0	-3.24
4.0	48.0	-8.84

TABLE 3D

Shutdown from 100% Full Power

δT(hours)	T(hours after shutdown)	-Reactivity (mk)
0.5	0.5	15.50
0.5	1.0	29.02
1.0	2.0	51.13
2.0	4.0	80.76
4.0	8.0	105.55
4.0	12.0	107.01
4.0	16.0	97.57
4.0	20.0	83.16
4.0	24.0	67.05
4.0	28.0	51.11
4.0	32.0	36.52

TABLE 3E

Theoretical Xenon Transient Following Shutdown from 100% FP

T(hours)	$C_x(t) \times 10^{-13}$ (cm^{-3})	-Reactivity (mk)	-Reactivity*
0.0	4.75	28.70	0.00
1.0	9.26	55.88	27.18
2.0	13.29	80.20	51.50
3.0	15.96	96.37	67.67
4.0	18.36	110.84	82.14
6.0	21.66	130.73	102.03
8.0	23.39	141.20	113.40
9.0	23.81	143.73	115.03
10.0	23.99	144.82	116.12
11.0	23.97	144.69	115.99
14.0	23.01	138.91	110.21
16.0	21.87	132.02	103.30
24.0	15.92	96.11	67.41
28.0	13.01	78.53	49.83
36.0	7.94	47.94	19.24
44.0	5.01	30.25	1.55

* See APPENDIX A (less reactivity by 28.7 mk equilibrium xenon).

TABLE 4A

Startup Transient to 100% FP

δT(hours)	T(hours after startup)	-Reactivity (mk)
0.5	0.5	1.49
0.5	1.0	2.87
1.0	2.0	5.40
2.0	4.0	9.73
4.0	8.0	16.03
4.0	12.0	20.12
4.0	16.0	22.78
4.0	20.0	24.51
4.0	24.0	25.64
4.0	28.0	26.38
4.0	32.0	26.87
4.0	36.0	27.19
4.0	40.0	27.40
4.0	44.0	27.53
4.0	48.0	27.62
4.0	52.0	27.68
4.0	56.0	27.72

TABLE 4B

Startup Transient to 90% FP

δT(hours)	T(hours after startup)	- Reactivity (mk)
0.5	0.5	1.39
0.5	1.0	2.72
1.0	2.0	5.21
2.0	4.0	9.51
4.0	8.0	15.82
4.0	12.0	19.92
4.0	16.0	22.61
4.0	20.0	24.35
4.0	24.0	25.48
4.0	28.0	26.22
4.0	32.0	26.70
4.0	36.0	27.02
4.0	40.0	27.22
4.0	44.0	27.36
4.0	48.0	27.45
4.0	52.0	27.51
4.0	56.0	27.54

TABLE 4C

Startup Transient to 85% FP

δT(hours)	T(hours after startup)	-Reactivity (mk)
0.5	0.5	1.33
0.5	1.0	2.63
1.0	2.0	5.09
2.0	4.0	9.38
4.0	8.0	15.70
4.0	12.0	19.80
4.0	16.0	22.50
4.0	20.0	24.20
4.0	24.0	25.40
4.0	28.0	26.12
4.0	32.0	26.60
4.0	36.0	26.92
4.0	40.0	27.12
4.0	44.0	27.26
4.0	48.0	27.35
4.0	52.0	27.41
4.0	56.0	27.44

TABLE 4D

Startup Transient to 75% FP

δT(hours)	T(hours after startup)	-Reactivity (mk)
.5	.5	1.19
.5	1.0	2.41
1.0	2.0	4.80
2.0	4.0	9.07
4.0	8.0	15.41
4.0	12.0	19.54
4.0	16.0	22.22
4.0	20.0	23.97
4.0	24.0	25.11
4.0	28.0	25.86
4.0	32.0	26.35
4.0	36.0	26.67
4.0	40.0	26.88
4.0	44.0	27.02
4.0	48.0	27.11
4.0	52.0	27.17
4.0	56.0	27.21

TABLE 4E

Startup Transient to 50% FP

δT(hours)	T(hours after startup)	-Reactivity (mk)
.5	.5	.86
.5	1.0	1.82
1.0	2.0	3.89
2.0	4.0	7.92
4.0	8.0	14.24
4.0	12.0	18.43
4.0	16.0	21.16
4.0	20.0	22.95
4.0	24.0	24.11
4.0	28.0	24.87
4.0	32.0	25.37
4.0	36.0	25.70
4.0	40.0	25.91
4.0	44.0	26.05
4.0	48.0	26.14
4.0	52.0	26.20
4.0	56.0	26.24

TABLE 4F

Startup Transient to 25% FP

δT(hours)	T(hours after startup)	-Reactivity (mk)
.5	.5	.46
.5	1.0	1.04
1.0	2.0	2.43
2.0	4.0	5.58
4.0	8.0	11.36
4.0	12.0	15.56
4.0	16.0	18.39
4.0	20.0	20.26
4.0	24.0	21.48
4.0	28.0	22.28
4.0	32.0	22.81
4.0	36.0	23.16
4.0	40.0	23.38
4.0	44.0	23.53
4.0	48.0	23.63
4.0	52.0	23.69
4.0	56.0	23.73

Power Setback Computations

TABLE 5A

Setback to 75% FP

δT(hours)	T(hours after setback)	-Reactivity (mk)
0.5	.5	3.055
0.5	1.0	4.58
1.0	2.0	5.57
2.0	4.0	5.088
4.0	8.0	3.35
4.0	12.0	2.12
4.0	16.0	1.27
4.0	20.0	0.68
4.0	24.0	0.28
4.0	28.0	0.021
4.0	32.0	-.15

TABLE 5B

Setback to 50% FP

δT(hours)	T(hours after setback)	-Reactivity (mk)
0.5	0.5	6.63
0.5	1.0	10.63
1.0	2.0	14.22
2.0	4.0	14.30
4.0	8.0	9.83
4.0	12.0	6.32
4.0	16.0	3.87
4.0	20.0	2.14
4.0	24.0	.93
4.0	28.0	.10
4.0	32.0	-.45

TABLE 5C

Setback to 25% FP

δT(hours)	T(hours after setback)	k_{eff} (milli-k)
0.5	0.5	10.75
0.5	1.0	18.56
1.0	2.0	28.07
2.0	4.0	33.43
4.0	8.0	26.85
4.0	12.0	18.10
4.0	16.0	11.32
4.0	20.0	6.77
4.0	24.0	3.52
4.0	28.0	1.15
4.0	32.0	-.56

TABLE 6

Startup Power from 1% FP as Function at Time

δT(s)	T(min)	Power(%FP)
0	0	1
60	1	4
20		7
20		10
20	2	13
8.6		16
8.6		19
8.6		22
8.6		25
8.6		28
8.6		31
8.6	3	34
10		37
10		40
10		43
10		46
10		49
10	4	52
10		55
10		58
10		61
10		64
10		67
10	5	70

TABLE 7

Reactivity and Power Transients (D&A Time)

δt(secs)	Power(%FP)	k_{eff} (milli-k)
0.71217 hrs (0)	1	21.90
60	4	22.31
20	7	22.44
20	10	22.56
20	13	22.66
8.6	16	22.70
8.6	19	22.73
8.6	22	22.76
8.6	25	22.78
8.6	28	22.80
8.6	31	22.81
8.6	34	22.82
10	37	22.82
10	40	22.82
10	43	22.81
10	46	22.80
10	49	22.77
10	52	

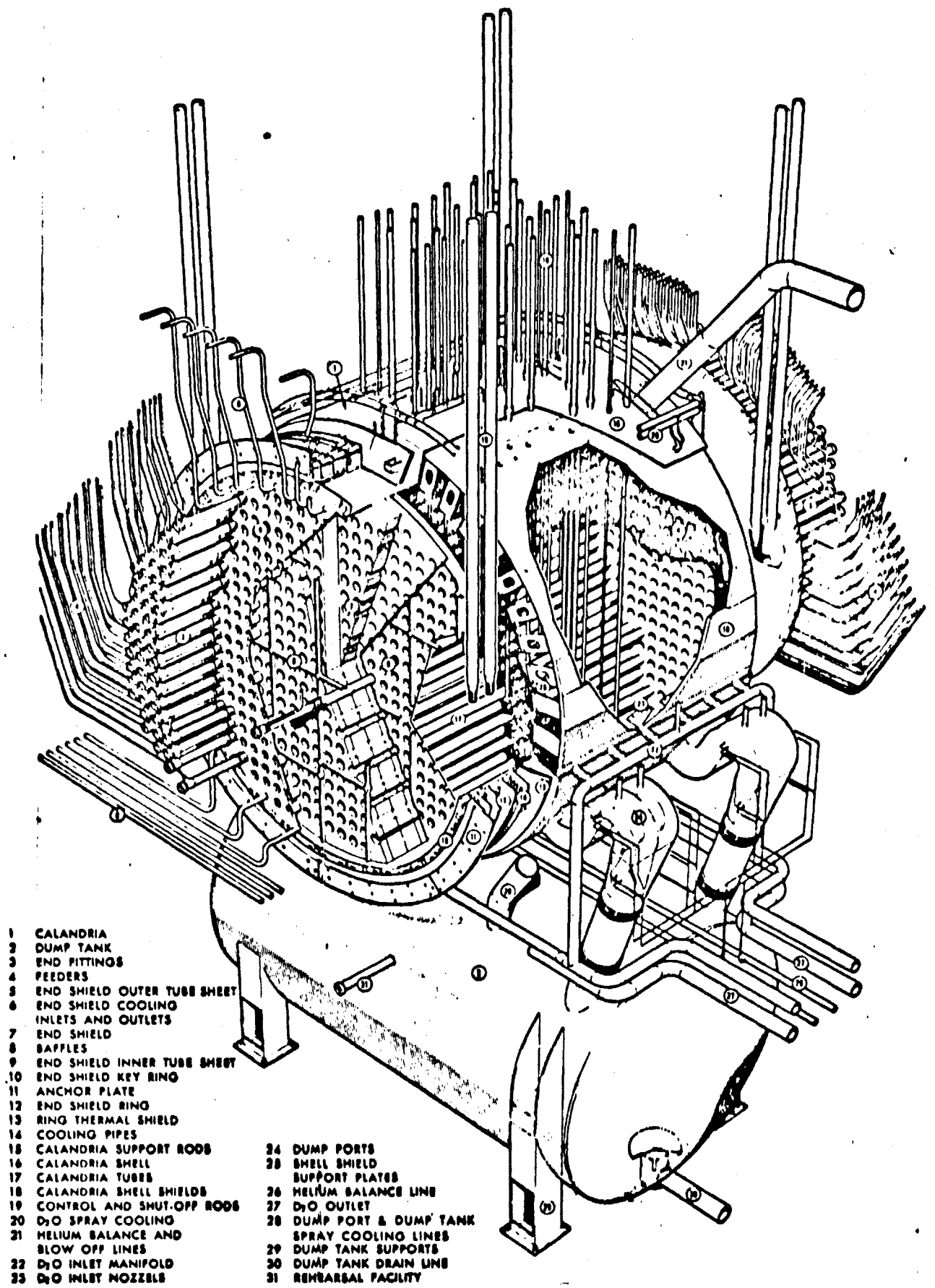

FIGURE 1 REACTOR ASSEMBLY

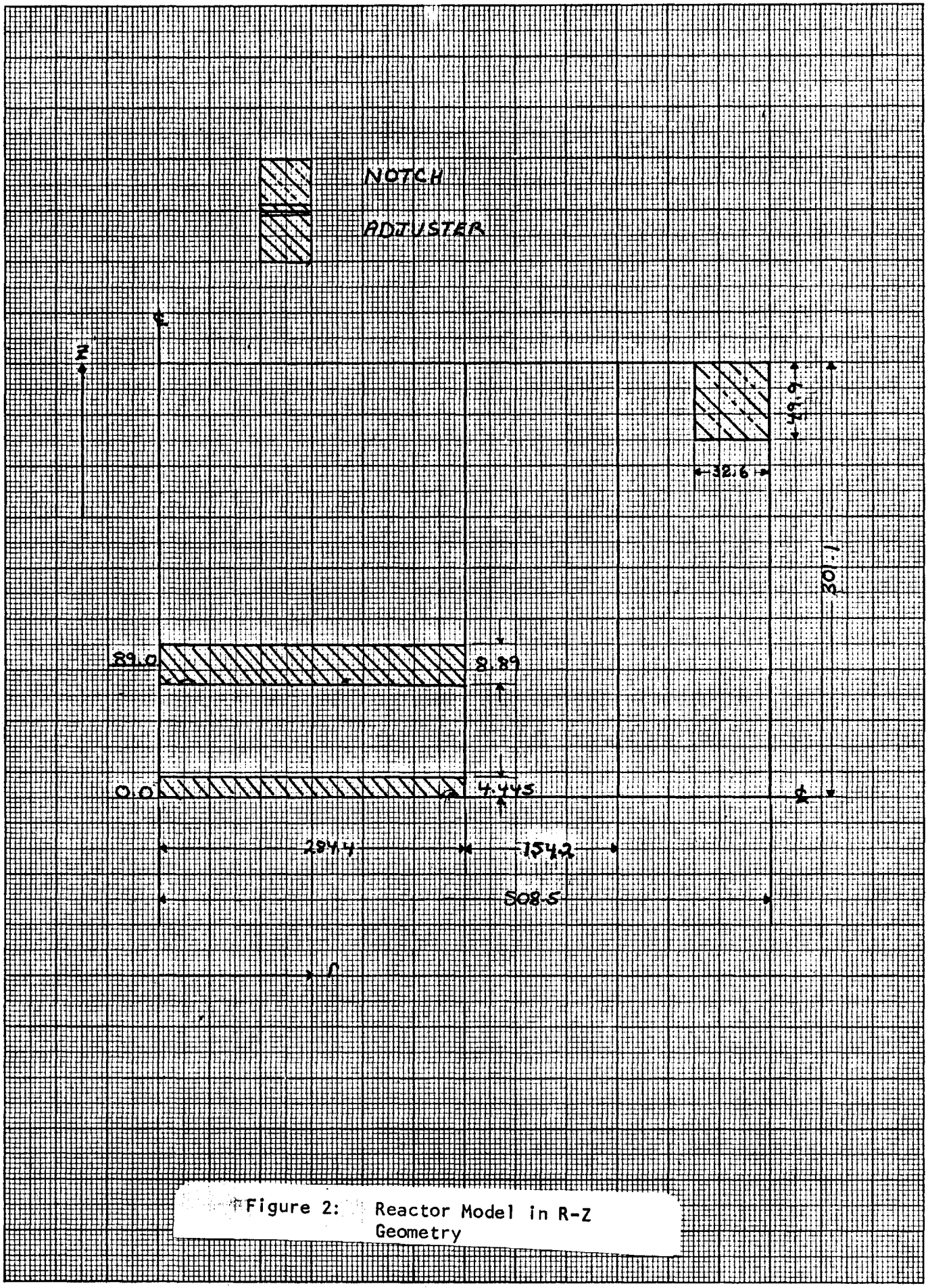

Figure 2: Reactor Model in R-Z Geometry

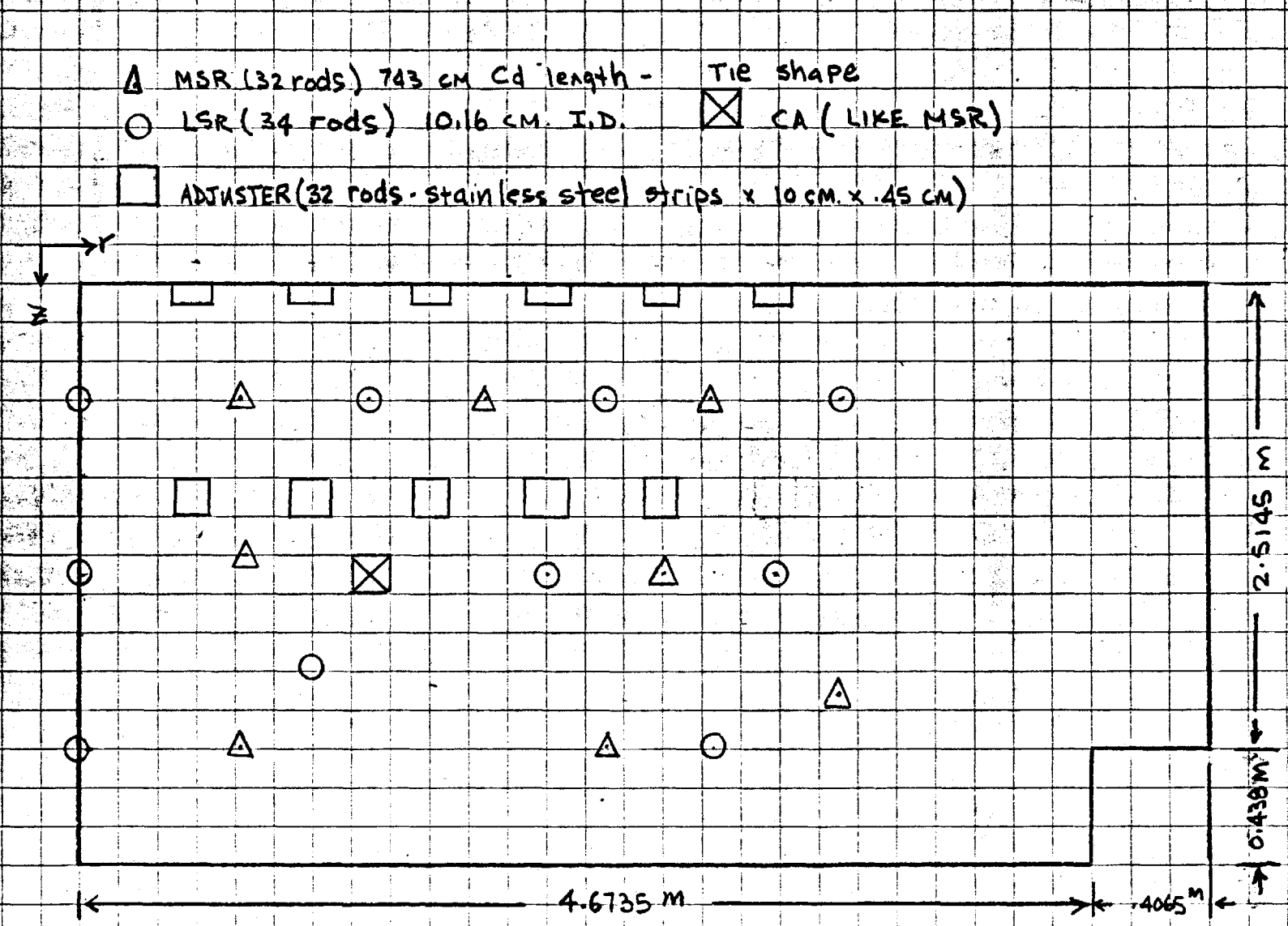

FIGURE 3 PLAN VIEW - 1/4 CORE REACTOR

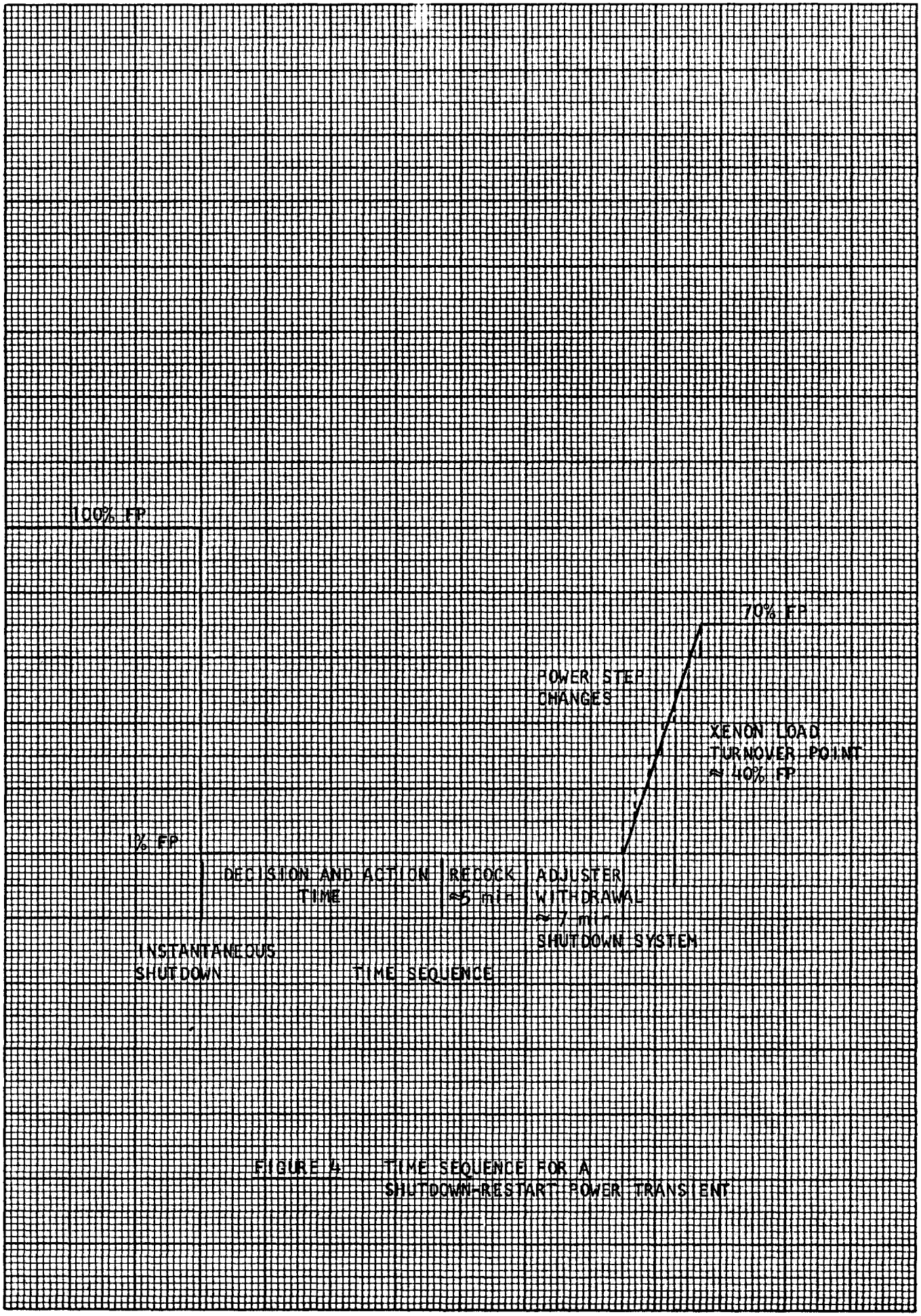

FIGURE 4 TIME SEQUENCE FOR A SHUTDOWN-RESTART POWER TRANSIENT

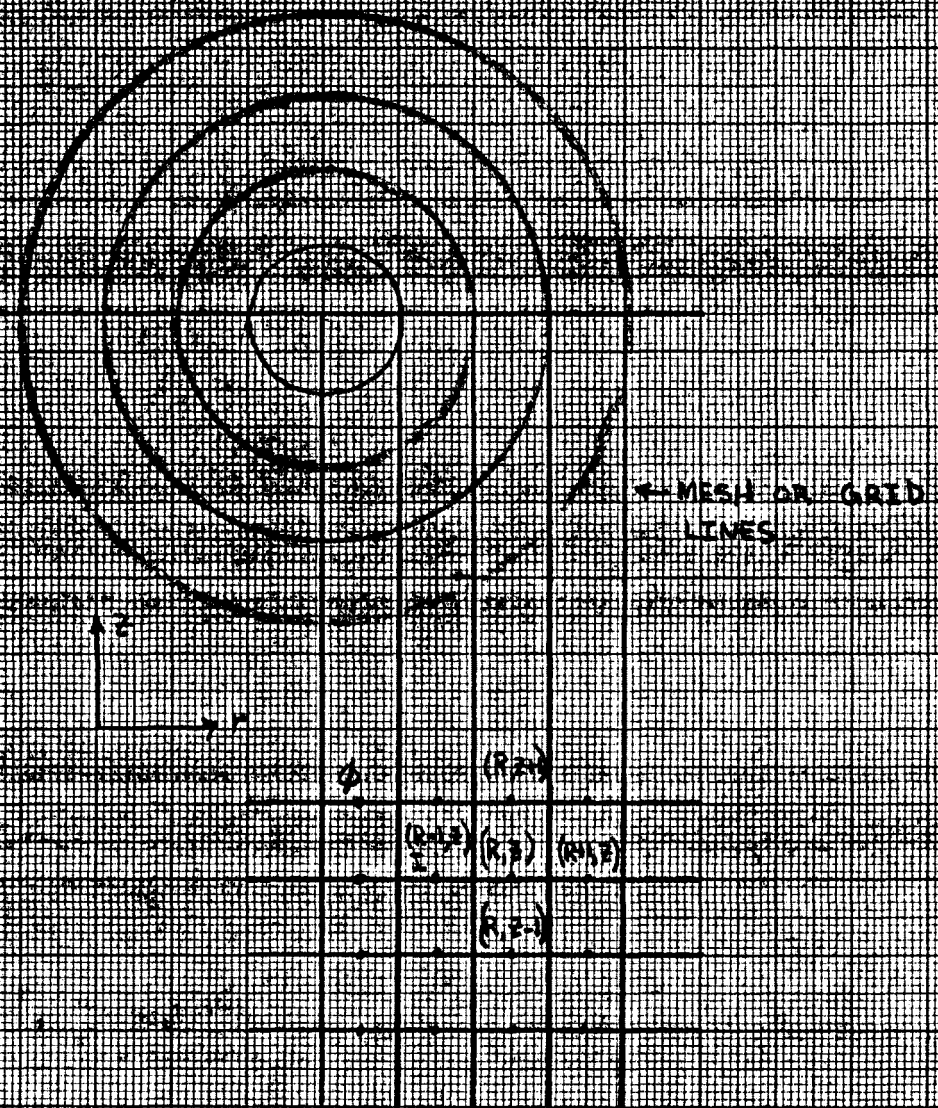

FIGURE 5. R-Z GEOMETRY OF GRID REPRESENTATION OF REACTOR

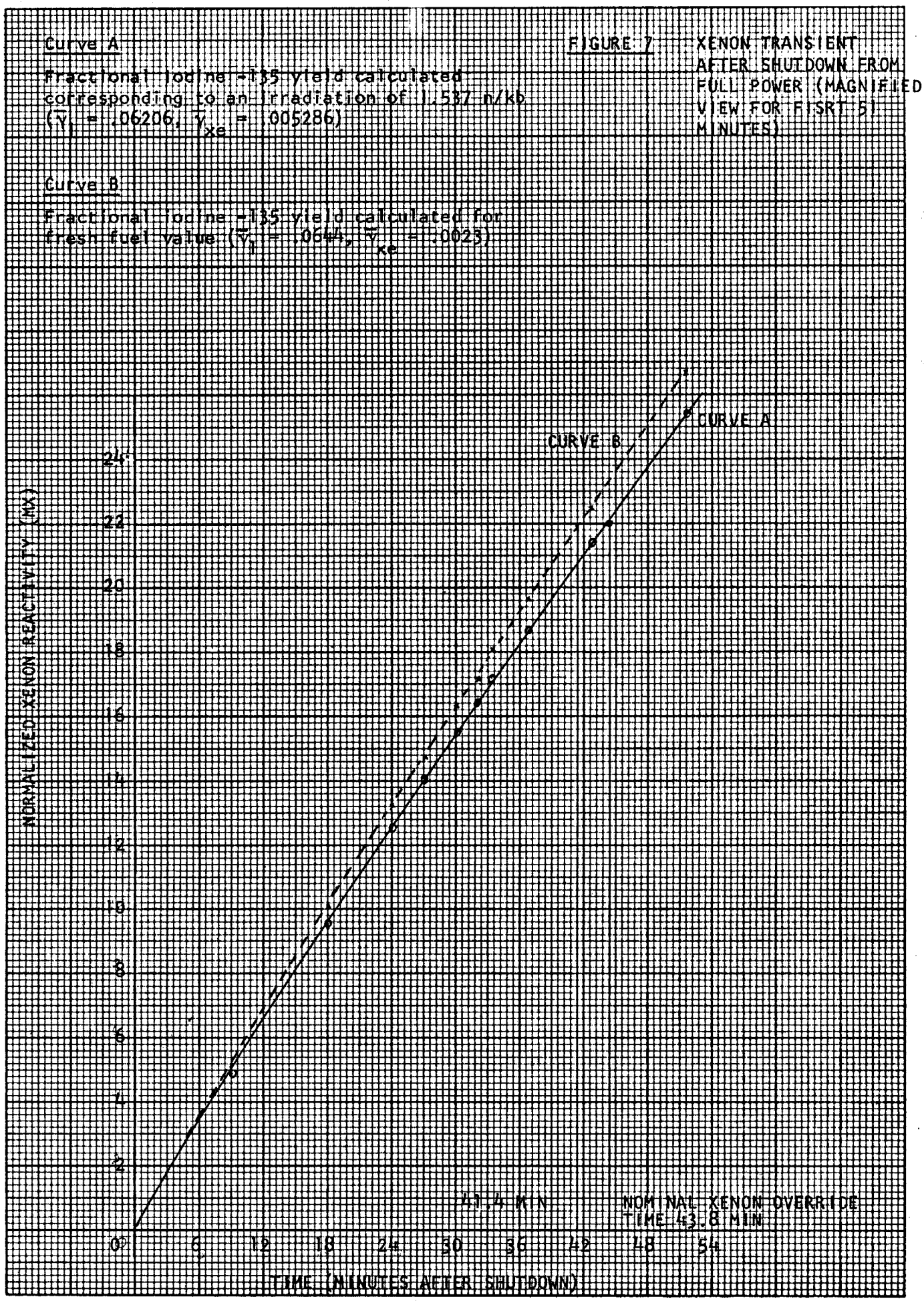
Curve A
Fractional Iodine-135 yield calculated corresponding to an irradiation of 1.587 n/kb ($\bar{\nu}_I$ = .06206, $\bar{\nu}_{Xe}$ = .005286)
Curve B
Fractional Iodine-135 yield calculated for fresh fuel value ($\bar{\nu}_I$ = .0644, $\bar{\nu}_{Xe}$ = .0023)
FIGURE 7 XENON TRANSIENT AFTER SHUTDOWN FROM FULL POWER (MAGNIFIED VIEW FOR FIRST 54 MINUTES)
CURVE A
CURVE B
NORMALIZED XENON REACTIVITY (MX)
TIME (MINUTES AFTER SHUTDOWN)
41.4 MIN
NOMINAL XENON OVERRIDE TIME 43.8 MIN
0
6
12
18
24
30
36
42
48
54
2
4
8
10
14
16
20
22
24

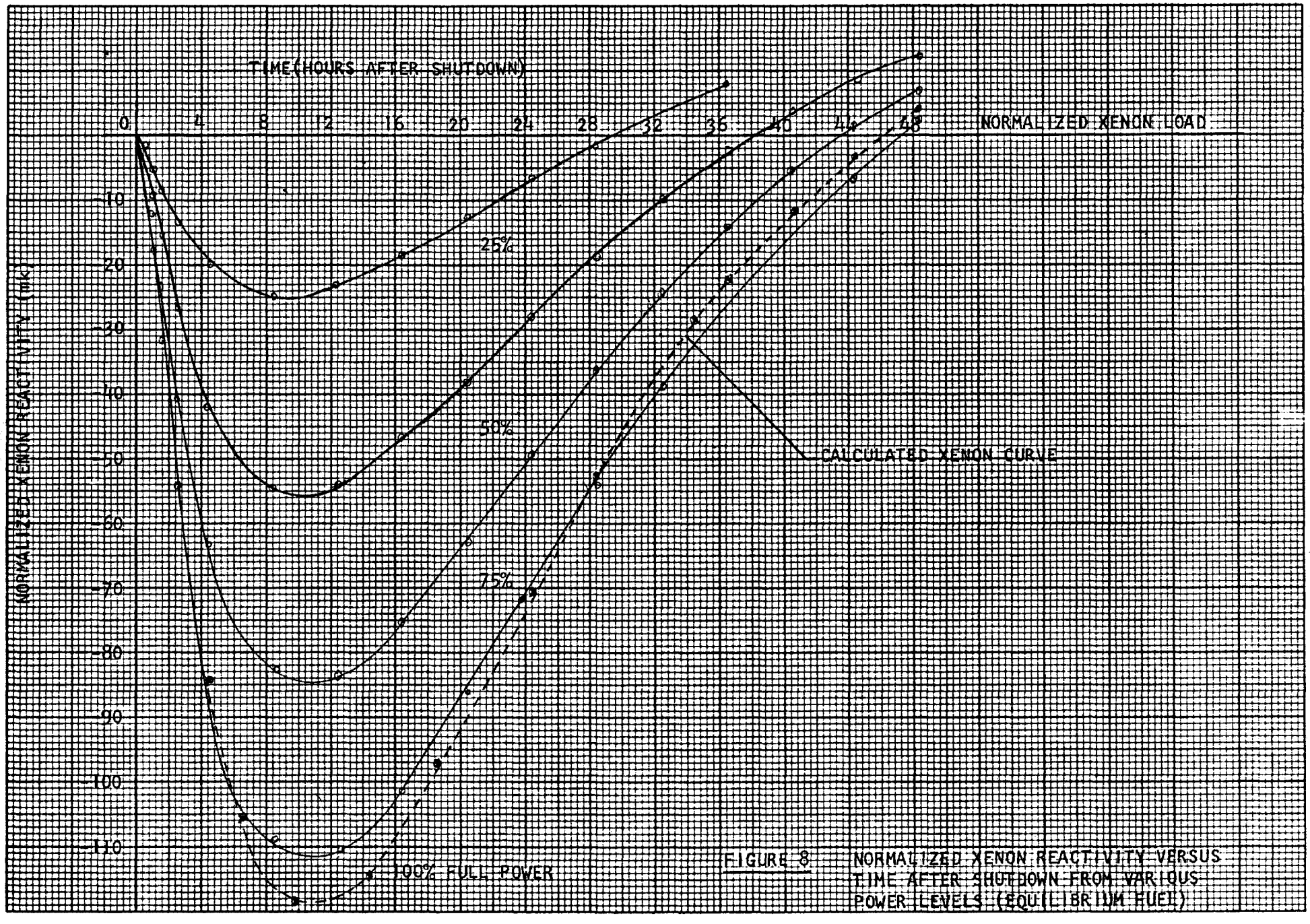

FIGURE 8 NORMALIZED XENON REACTIVITY VERSUS TIME AFTER SHUTDOWN FROM VARIOUS POWER LEVELS (EQUILIBRIUM FUEL)

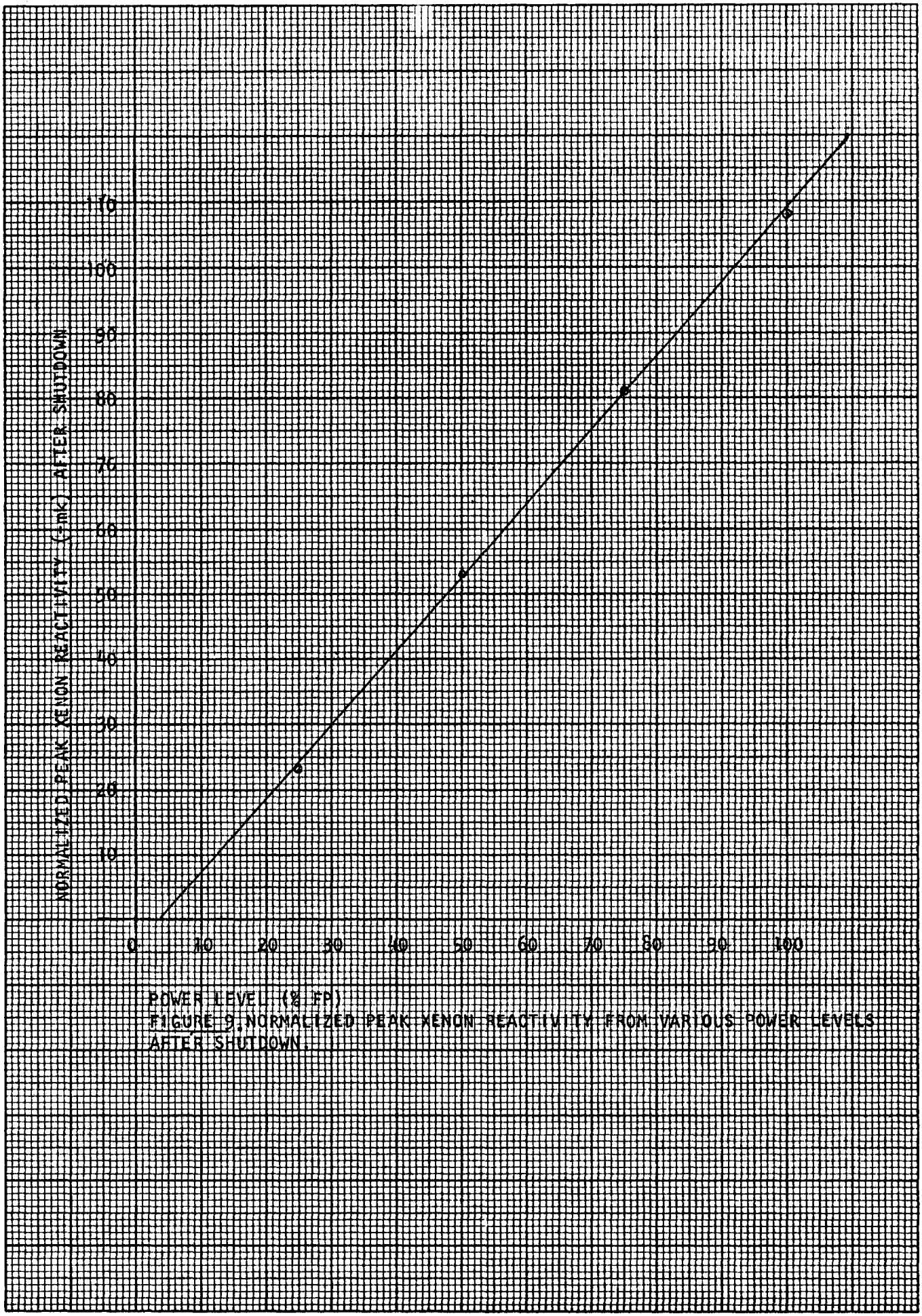

FIGURE 9. NORMALIZED PEAK XENON REACTIVITY FROM VARIOUS POWER LEVELS AFTER SHUTDOWN.

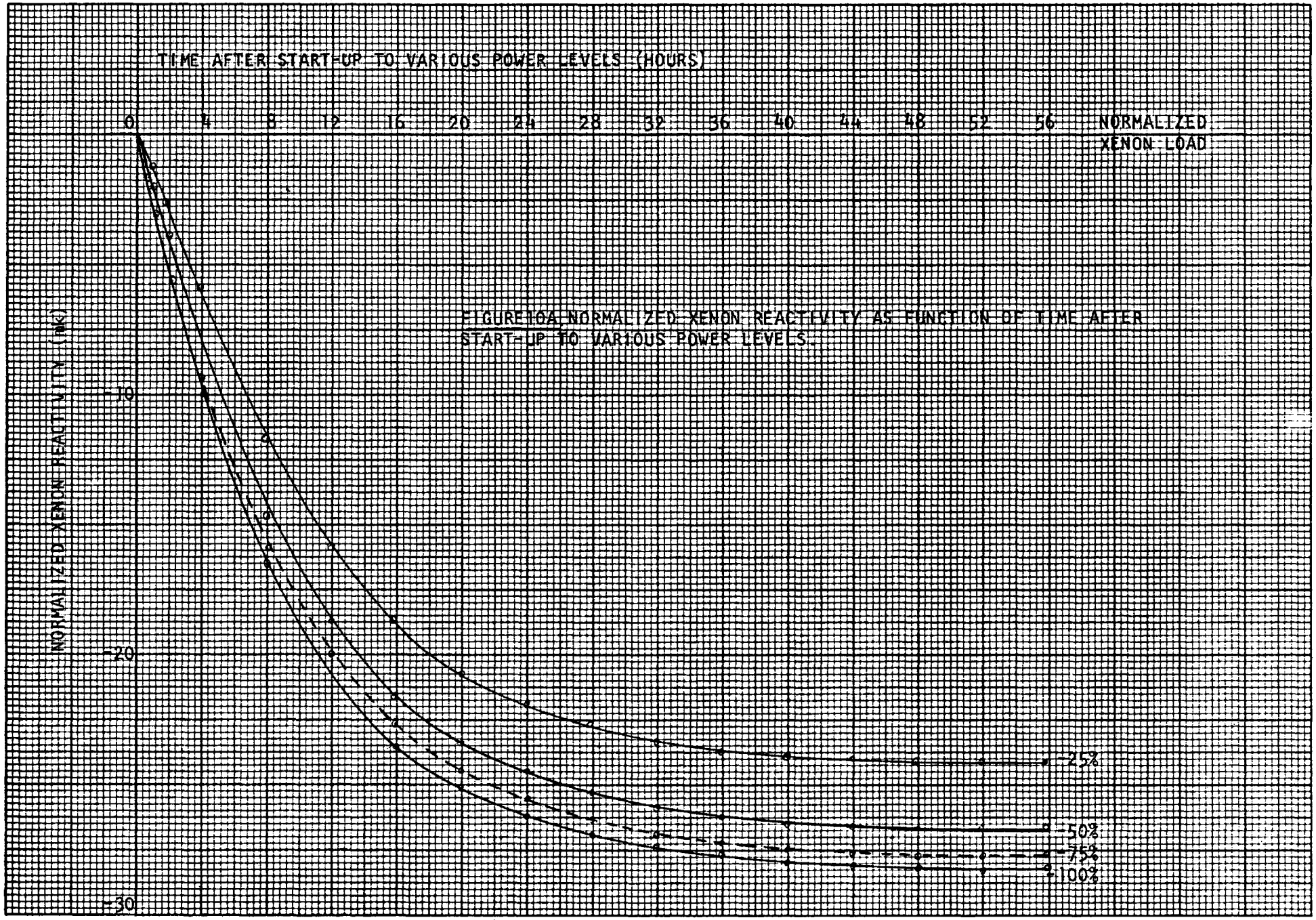

FIGURE 16A NORMALIZED XENON REACTIVITY AS FUNCTION OF TIME AFTER START-UP TO VARIOUS POWER LEVELS.

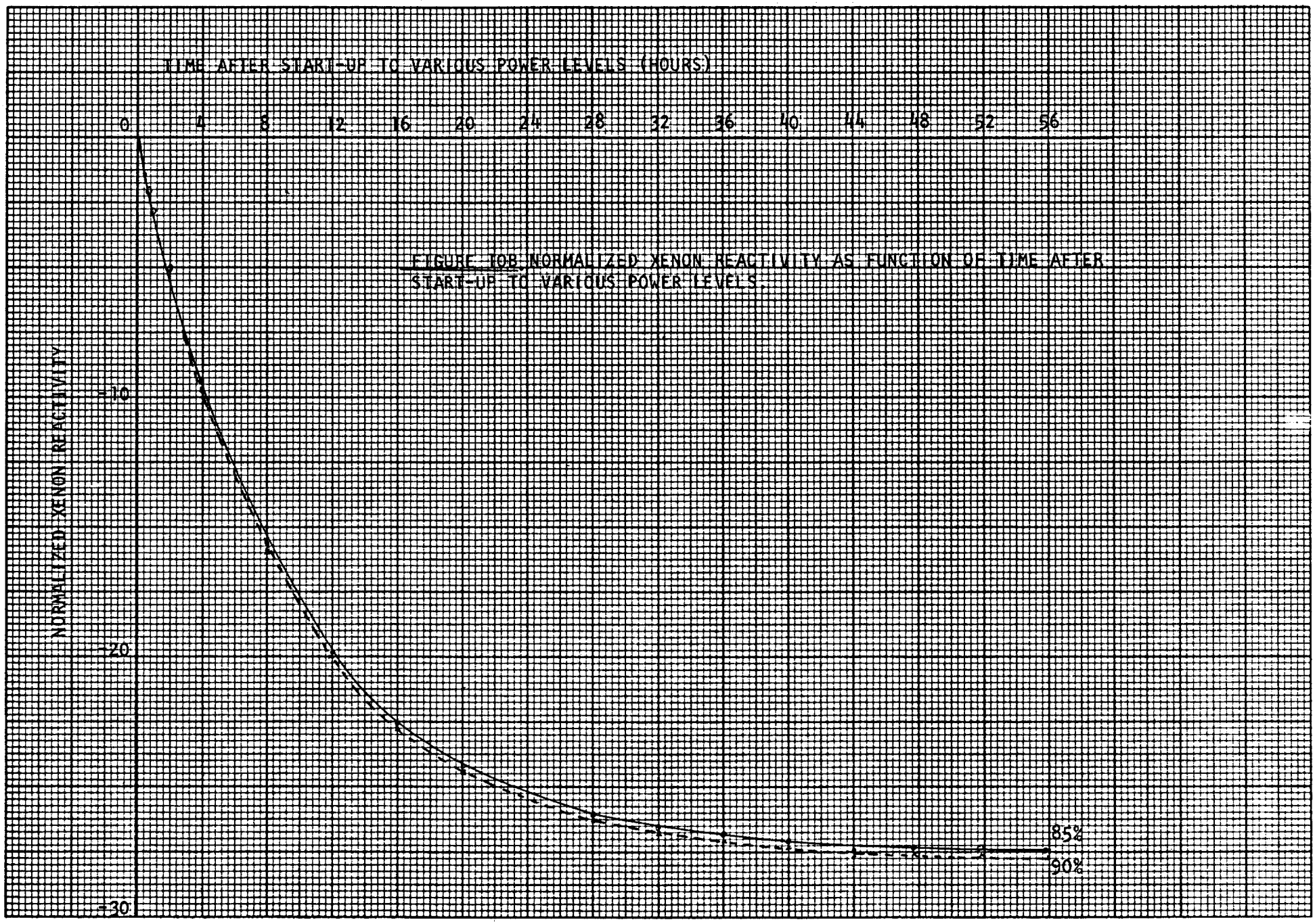

FIGURE 10B NORMALIZED XENON REACTIVITY AS FUNCTION OF TIME AFTER START-UP TO VARIOUS POWER LEVELS.

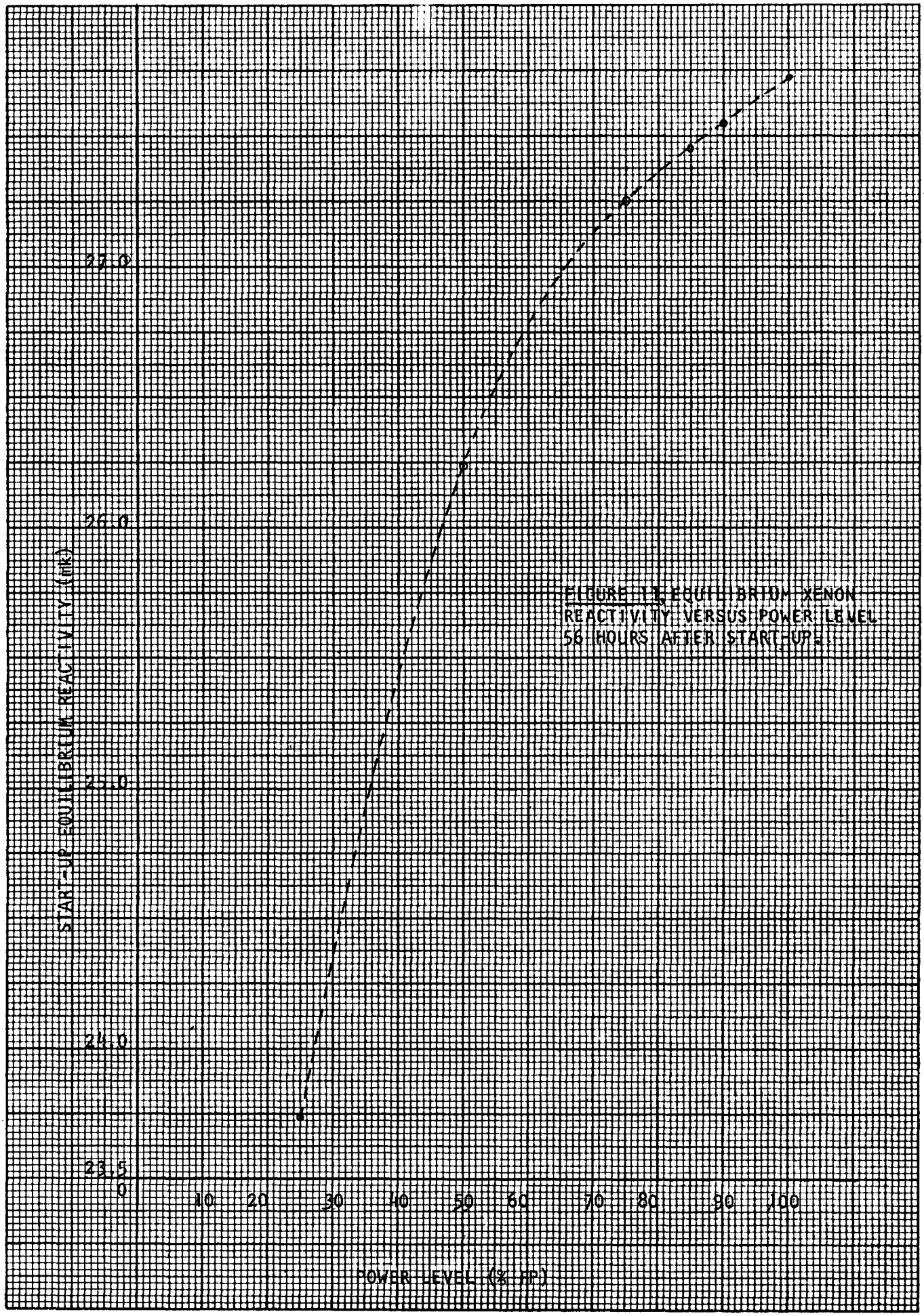

FIGURE 13 EQUILIBRIUM XENON REACTIVITY VERSUS POWER LEVEL 56 HOURS AFTER START-UP

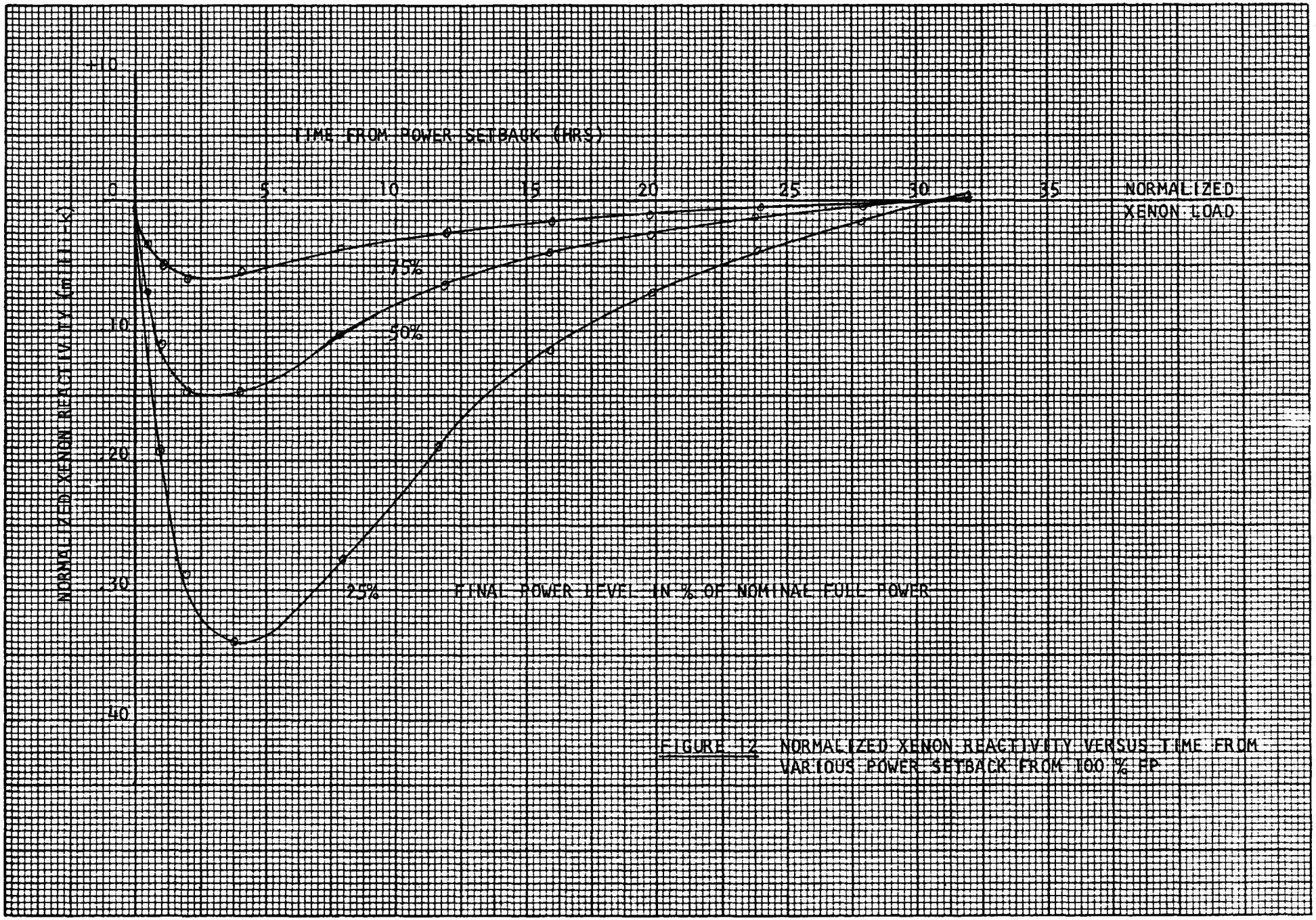

FIGURE 12 NORMALIZED XENON REACTIVITY VERSUS TIME FROM VARIOUS POWER SETBACK FROM 100 % FP

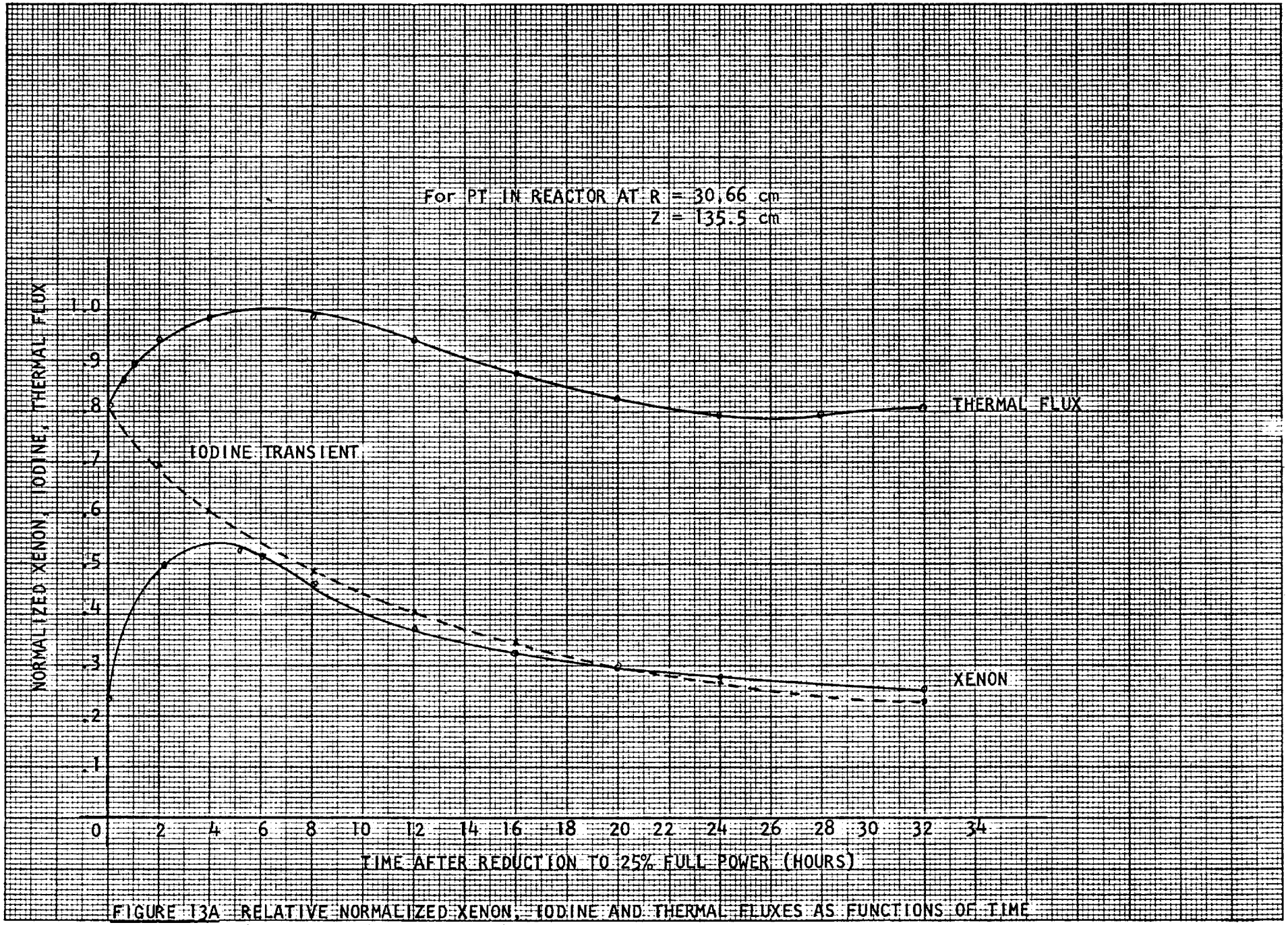

FIGURE 13A RELATIVE NORMALIZED XENON, IODINE AND THERMAL FLUXES AS FUNCTIONS OF TIME (FOR REDUCTION TO 25% FP)

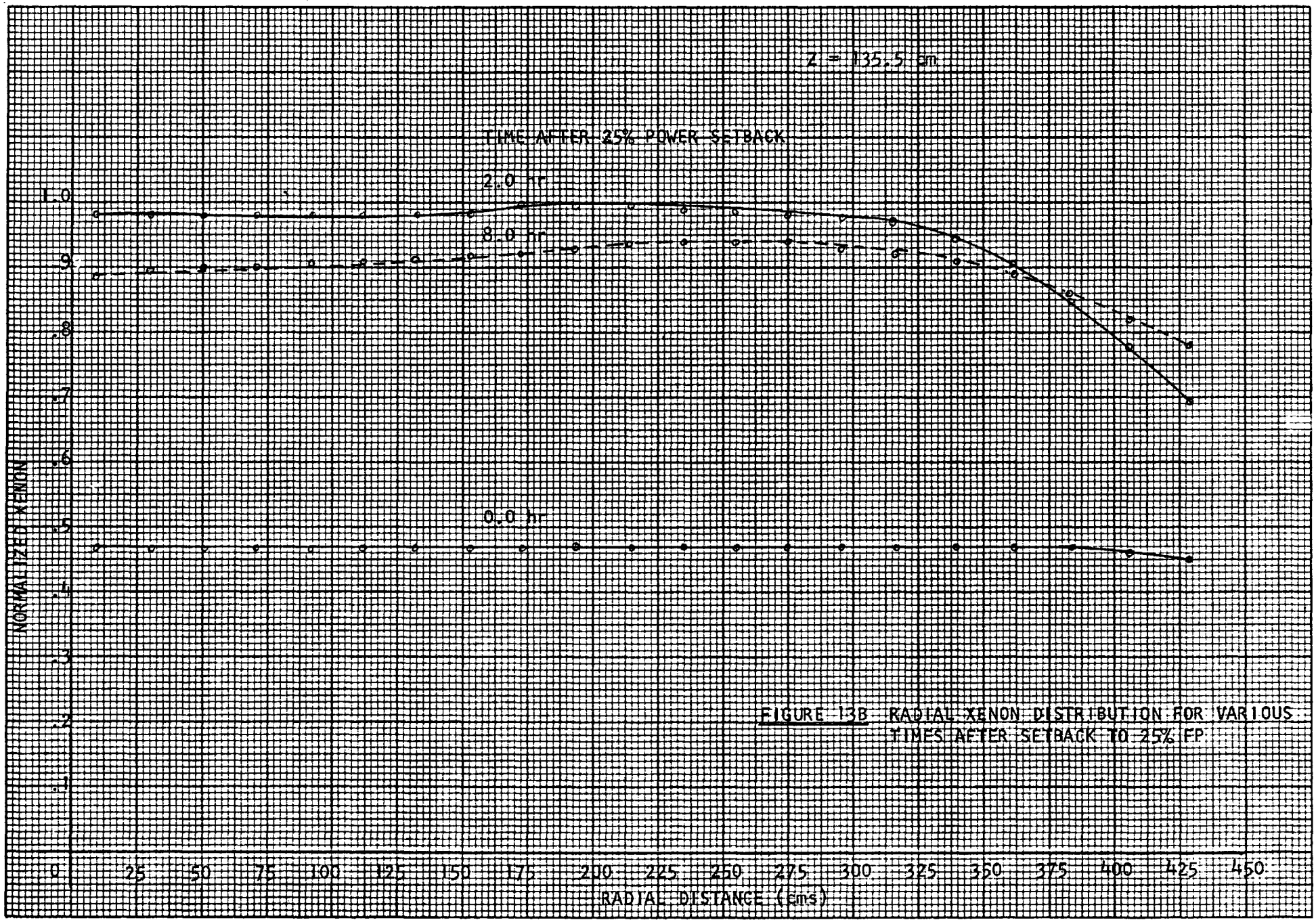

FIGURE 13B RADIAL XENON DISTRIBUTION FOR VARIOUS TIMES AFTER SETBACK TO 25% FP

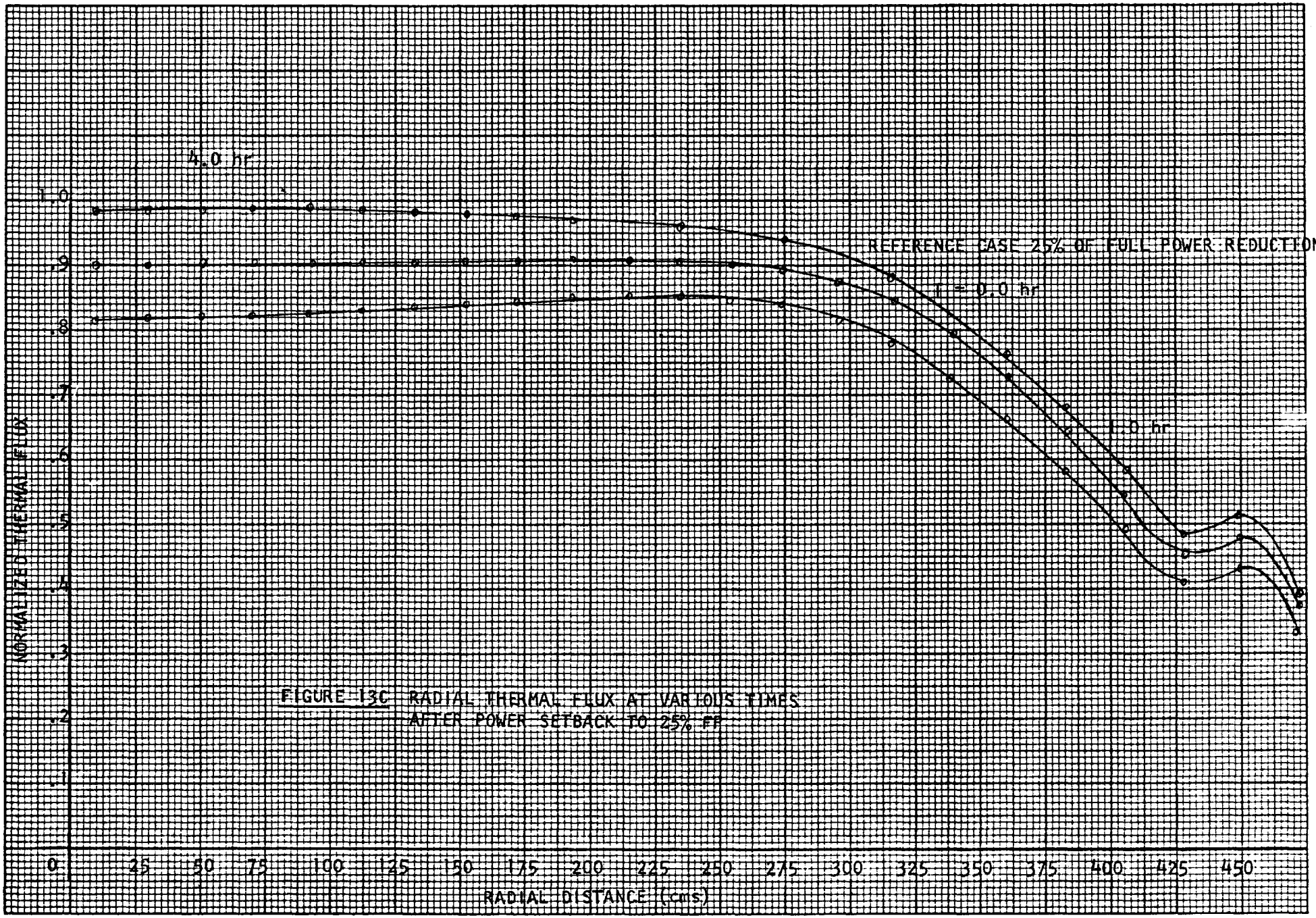

FIGURE 13C RADIAL THERMAL FLUX AT VARIOUS TIMES AFTER POWER SETBACK TO 25% FP

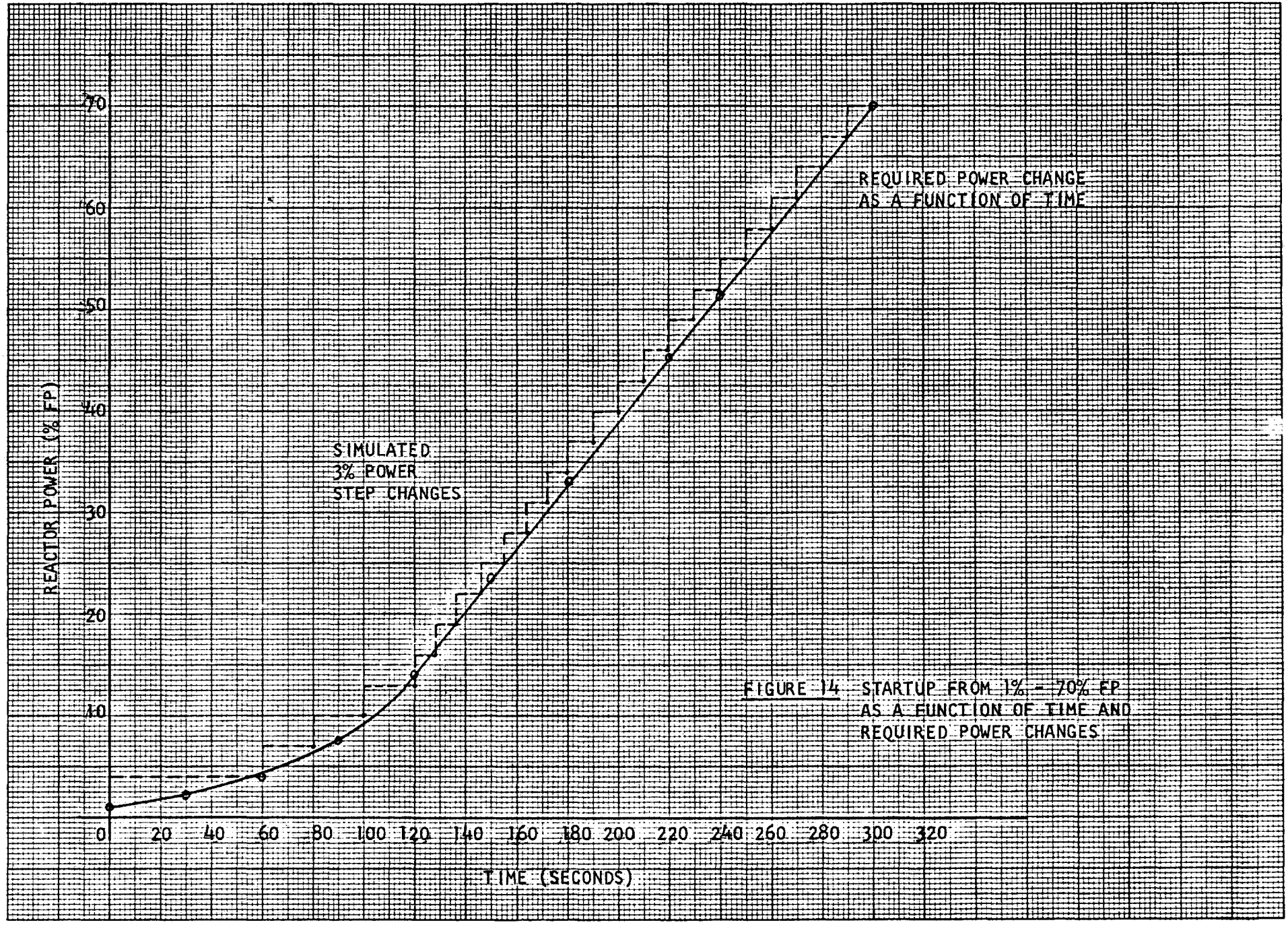

FIGURE 14 STARTUP FROM 1% - 70% FP AS A FUNCTION OF TIME AND REQUIRED POWER CHANGES

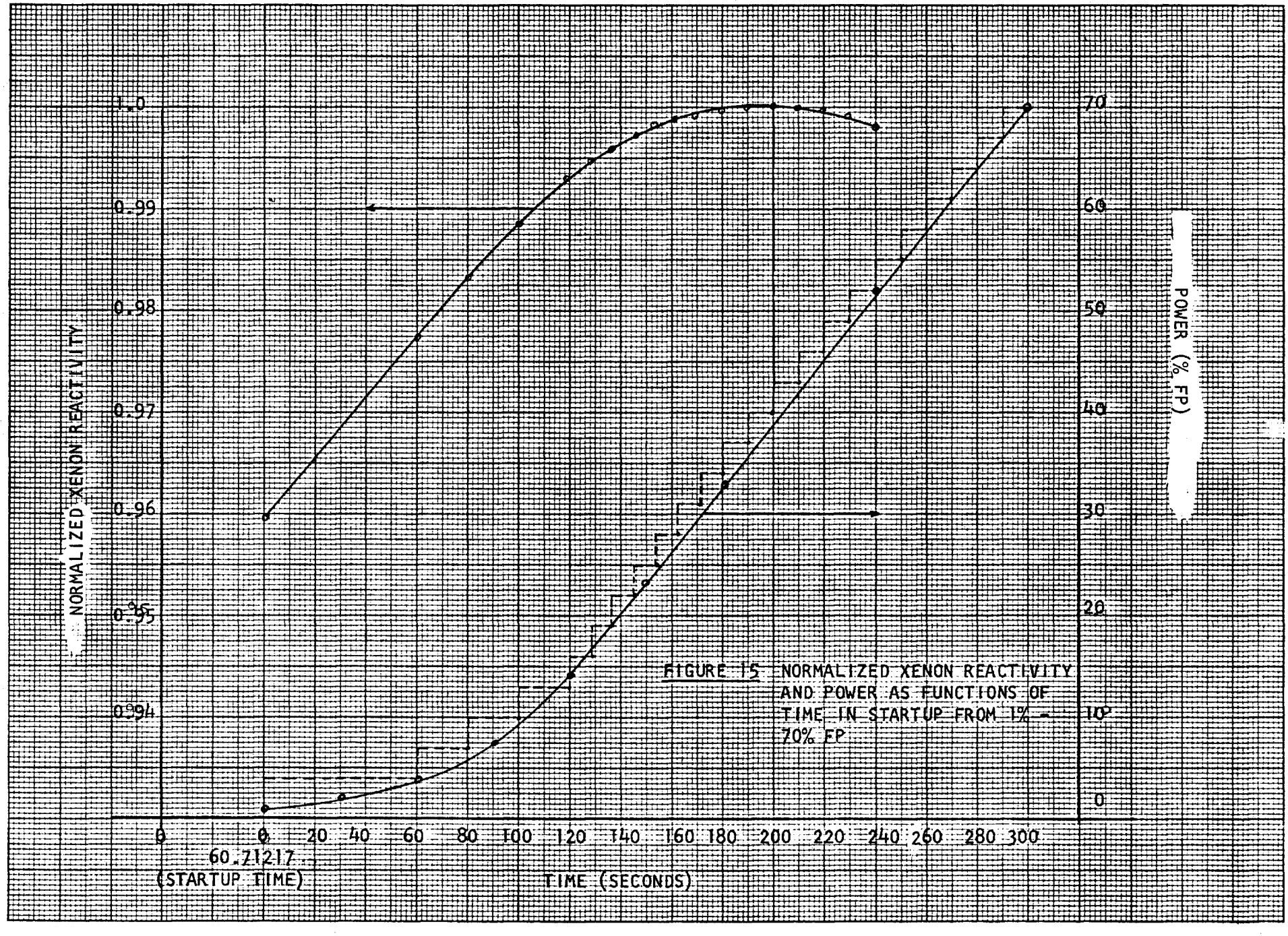

FIGURE 15 NORMALIZED XENON REACTIVITY AND POWER AS FUNCTIONS OF TIME IN STARTUP FROM 1% - 70% FP

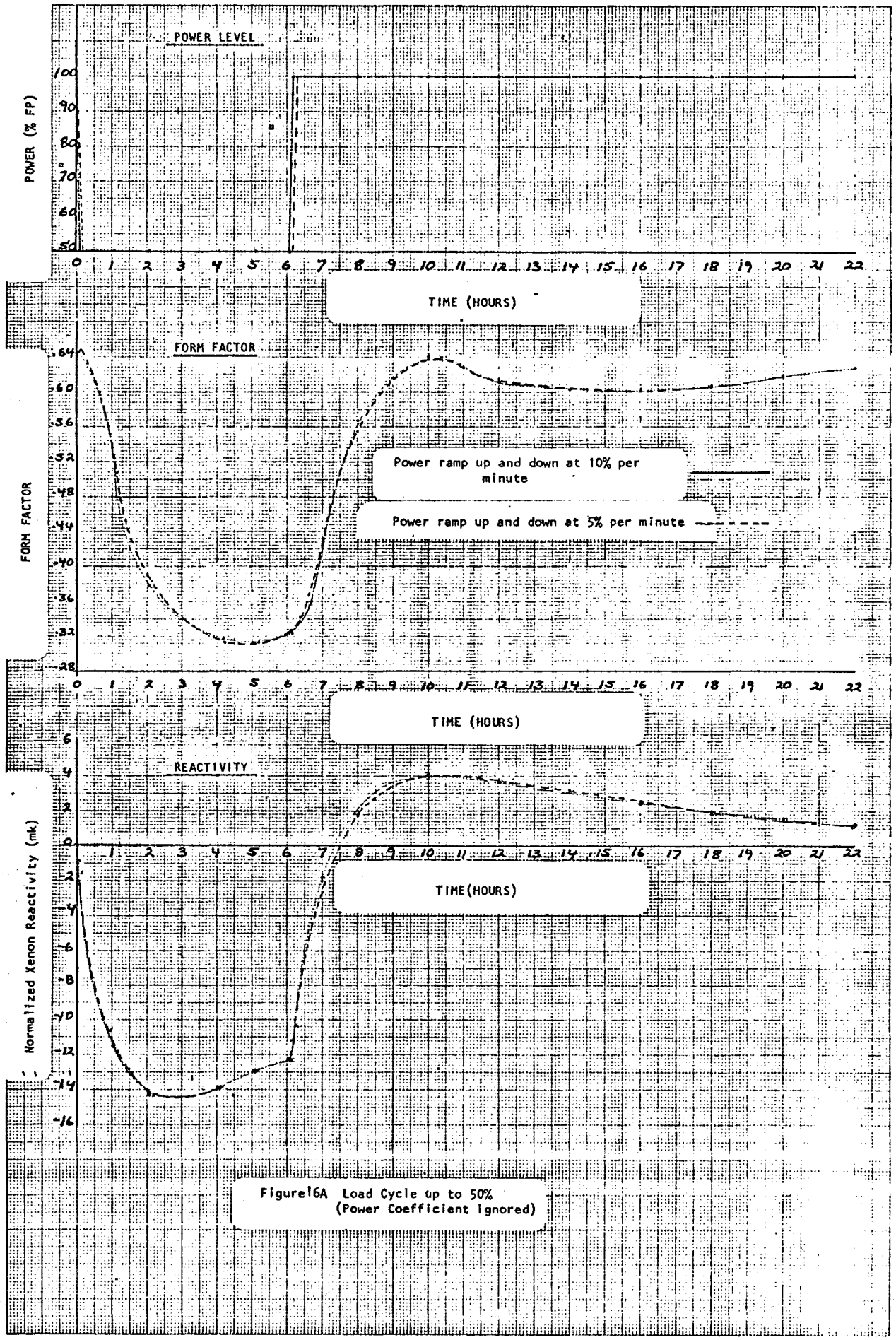

Figure16A Load Cycle up to 50%
(Power Coefficient Ignored)

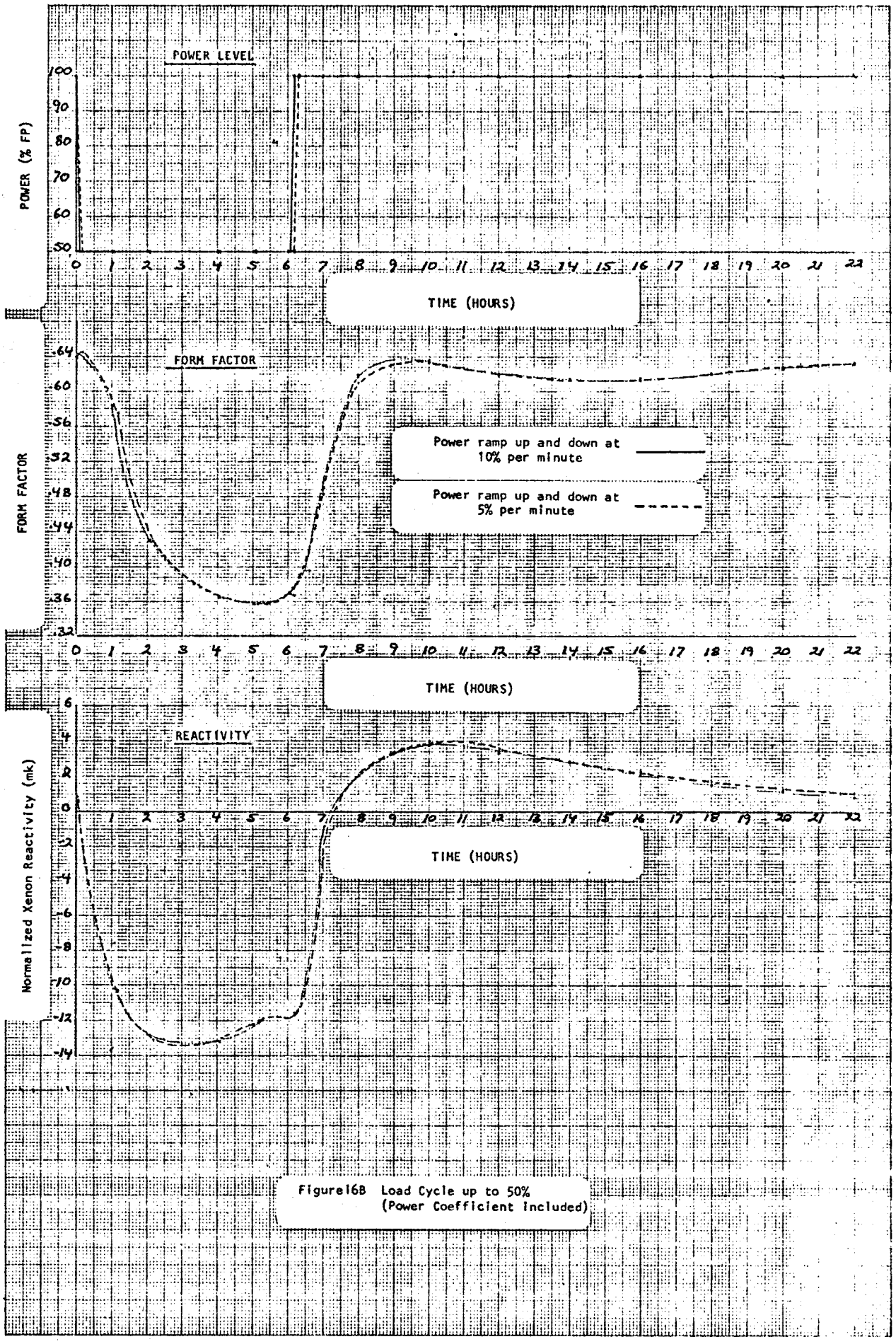

Figure16B Load Cycle up to 50%
(Power Coefficient Included)

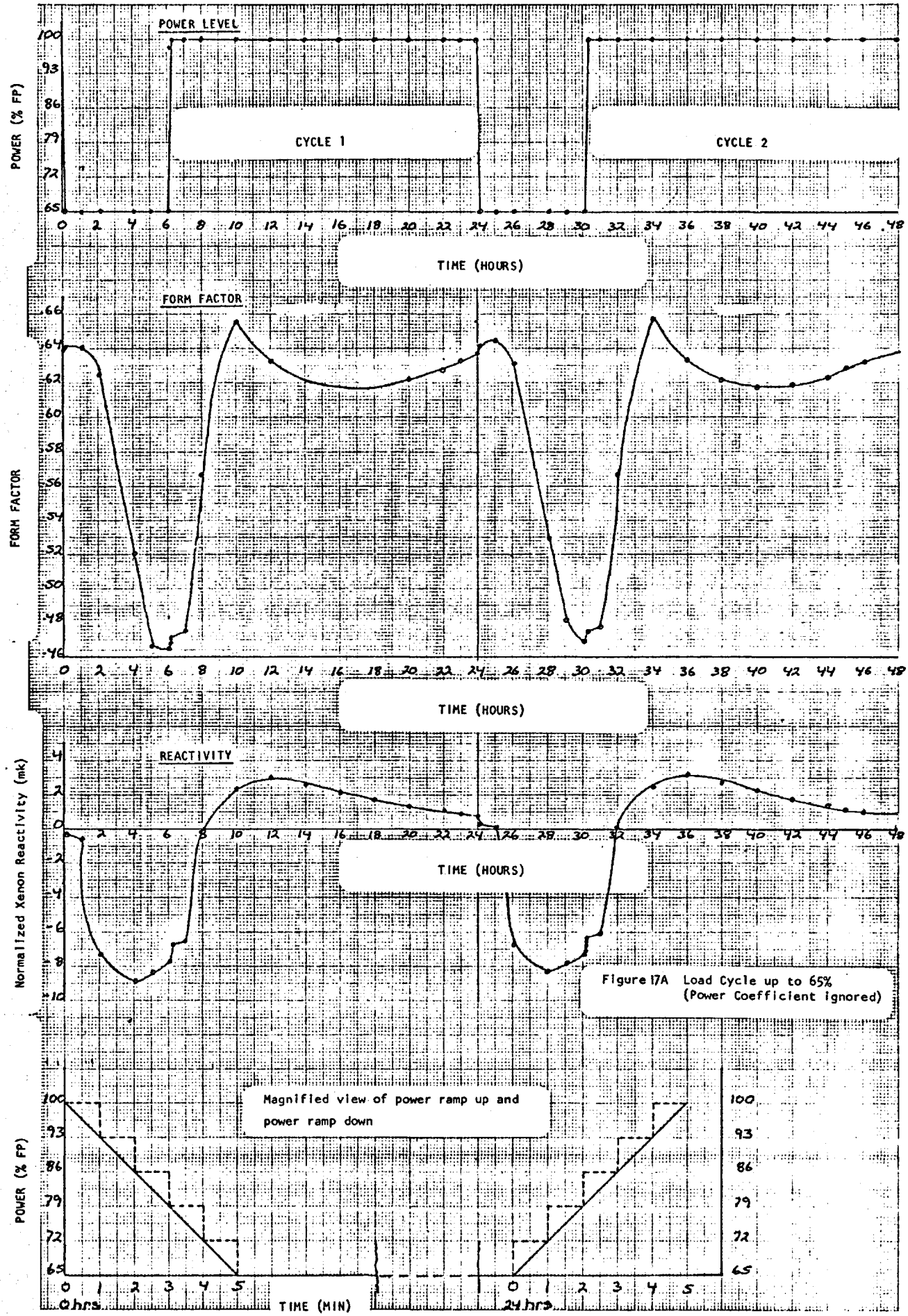

Figure 17A Load Cycle up to 65%
(Power Coefficient ignored)

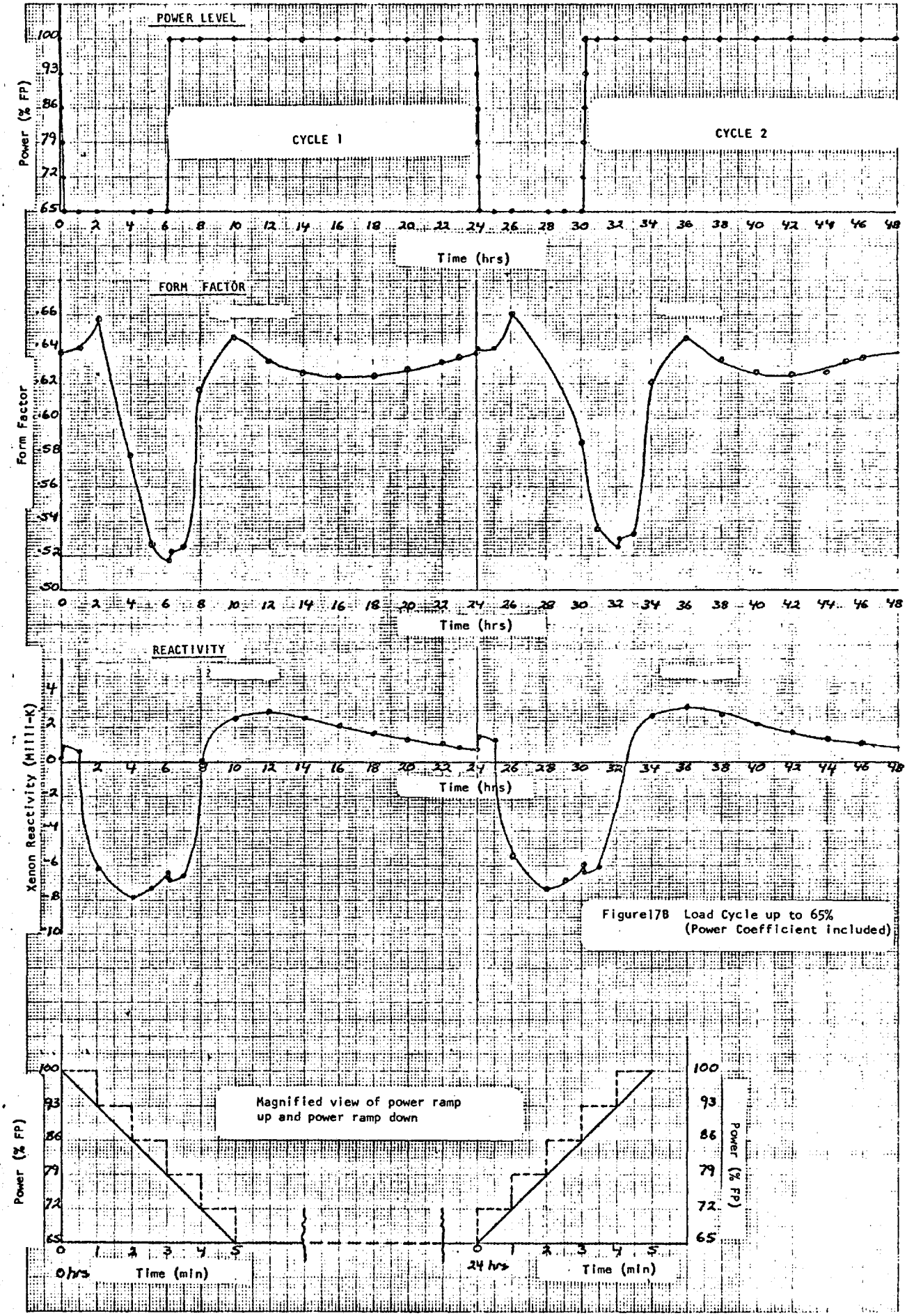

Figure17B Load Cycle up to 65% (Power Coefficient included)

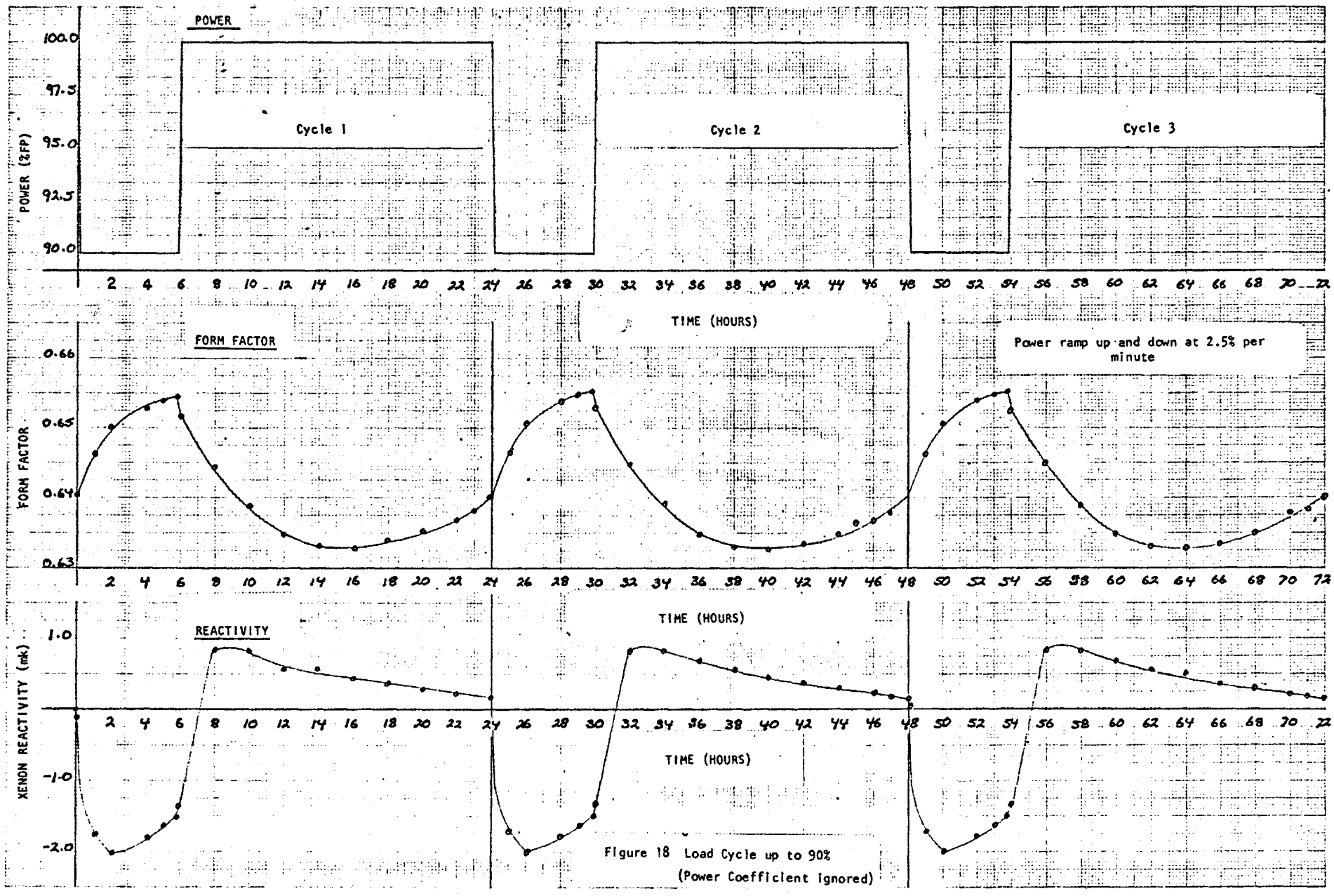

Figure 18 Load Cycle up to 90%
(Power Coefficient Ignored)

REFERENCES

1. Stacey, Weston M., "Space-Time Nuclear Reactor Kinetics", Academic Press, New York, 1969, Chapter 5.

2. Hughes, D.J. and R.B. Schwartz, "Neutron Cross Sections", BNL, New York, 1958.

3. AECL, private Communication.

4. ORNL Report, "2-D, 2-Gp Neutron Diffusion Code for IBM-7090 Computer", ORNL-3199, 1962.

5. CRRP-1151, "A G-20 Program For Studying Xenon Spatial Oscillations and Application to CANDU", July, 1963.

6. Harms, A.A., "An Introduction to the CANDU Nuclear Energy Conversion System", McMaster University, 1975.

7. Foster, A.R. and R.L. Wright, "Basic Nuclear Engineering", Allyn and Bacon, Inc., Boston, 1973.

8. Glasstone, S. and M.C. Edlund, "The Elements of Nuclear Reactor Theory", D. Van Nostrand Company, Inc., Princeton, 1952, Chapter 11.